

Pattern formation in generalized Turing systems

I. Steady-state patterns in systems with mixed boundary conditions

R. Dillon^{1,*}, P. K. Maini^{1,2}, H. G. Othmer^{1,*}

¹ Department of Mathematics, University of Utah, Salt Lake City, UT 84112, USA

² Centre for Mathematical Biology, Mathematical Institute, 24-29 St. Giles', Oxford OX1 3LB, UK

Received 13 October 1992; received in revised form 2 March 1993

Abstract. Turing's model of pattern formation has been extensively studied analytically and numerically, and there is recent experimental evidence that it may apply in certain chemical systems. The model is based on the assumption that all reacting species obey the same type of boundary condition pointwise on the boundary. We call these scalar boundary conditions. Here we study mixed or nonscalar boundary conditions, under which different species satisfy different boundary conditions at any point on the boundary, and show that qualitatively new phenomena arise in this case. For example, we show that there may be multiple solutions at arbitrarily small lengths under mixed boundary conditions, whereas the solution is unique under homogeneous scalar boundary conditions. Moreover, even when the same solution exists under scalar and mixed boundary conditions, its stability may be different in the two cases. We also show that mixed boundary conditions can reduce the sensitivity of patterns to domain changes.

Key words: Spatial pattern formations – Bifurcation – Turing systems

1 Introduction

It is well known in developmental biology that the fate of a cell in a developing or regenerating organism is often determined not only by its genome, but also by its location relative to other cells. Thus the orderly specialization of cell structure and function and the arrangement of cells into tissues and organs require mechanisms

* Supported in part by NIH Grant #GM29123

for the spatial and temporal control of cellular activity. The simplest aspect of this problem concerns pattern formation in an assemblage of essentially identical cells. One of the current hypotheses is that pattern formation results from the response of individual cells to an underlying spatial pattern of one or more chemical species called morphogens, and a major problem is to discover mechanisms by which the spatial pattern of the morphogens can be generated and maintained. Wolpert's concept of positional information [36] abstracted and formalized from earlier theories [12, 13, 7] the notion that a cell in a developing or regenerating system must "know" where it is relative to other cells in order to adopt the appropriate developmental pathway. In this approach, the question of pattern formation becomes that of discovering schemes that generate positional information.

A number of models for pattern formation and regulation are based on the hypothesis that a diffusible morphogen supplies positional information that can be interpreted by the cells. Such models fall into two main classes: source-sink models and Turing models. In source-sink models, specialized cells located at the boundary of the developmental field maintain the concentration of the morphogen at fixed levels. In a one-dimensional system of about 1 mm in length, a linear concentration distribution can be established in the time that is normally available for commitment to differentiation [37, 9]. Given fixed thresholds between different cell types, the tissue can be proportioned into any number of cell types in a perfectly scale-invariant way. There are, however, two facts which limit the applicability of this type of mechanism. While there are numerous systems that have one 'organizer' region that could serve as a source (or sink), such as the tip in the slug stage of *Dictyostelium discoideum* or the ZPA in the avian limb bud, the simultaneous occurrence of two such regions at opposite ends of a developmental axis is apparently rare. Secondly, the homeostatic mechanism that maintains the boundary concentrations at fixed levels must be able to vary the production or consumption of morphogen over a wide range. For instance, if the ends are held at c_0 and c_1 respectively, then the morphogen distribution is given by $c(x) = (c_1 - c_0)(x/L) + c_0$, and so the flux through the system must vary as $1/L$.

Turing models [34] involve two or more morphogens that react together and diffuse throughout the system. In Turing's original analysis no cells were distinguished a priori; all could serve as sources or sinks of the morphogen. Moreover, Turing only considered periodic systems or closed surfaces, in which case no boundary conditions are needed. More generally, we call any system of reaction-diffusion equations for which the boundary conditions are of the same type for all species a Turing system. In certain situations to be discussed in detail later, a spatially-homogeneous stationary state can, as a result of slow variation in parameters such as kinetic coefficients, become unstable with respect to small nonuniform disturbances. Such instabilities, which Turing called symmetry-breaking because the homogeneous locally-isotropic stationary state becomes unstable and therefore physically inaccessible, can lead to either a spatially nonuniform stationary state or to more complicated dynamical behavior. Such transitions from uniform stationary states to spatially- and/or temporally-ordered states might in turn lead, via an unspecified 'interpretation' mechanism, to spatially-ordered differentiation. For mathematical simplicity most analyses of Turing models deal with instabilities of uniform stationary states, since numerical analysis is generally required for more general reference states. However, Turing himself recognized the biological unreality of this in stating that 'most of an organism, most of the time is developing from one pattern to another, rather than from homogeneity into a pattern' [34].

Gradient models and reaction-diffusion models have been proposed to account for segmentation patterns along the antero-posterior axis of insects. However there are instances in which positional information models based on a simple “reading off” of morphogen concentration are clearly not sufficient to describe the results of observations. For example, in *Oncopeltus*, Wright and Lawrence [38] found that if cells that were not normally neighbours were juxtaposed by surgical manipulation, then a segment boundary would form at the interface when confronting cells came from sufficiently disparate positions in the antero-posterior axis of the same segment, and otherwise the segment simply regenerated normally. The latter result could be explained by the diffusive smoothing of a gradient, but the former requires the generation of the extreme positional values that specify the segmental boundary and these could not arise from a simple gradient mechanism. In *Drosophila*, surgical manipulation [15] or gene mutation can lead to deletions and mirror symmetrical duplications along the antero-posterior axis on length scales ranging from half the egg to within segments (see [16] for review). These results cannot be fully explained by a simple gradient model.

Reaction diffusion systems have been proposed to account for spatial pattern formation in several other biological systems and in chemical systems, but in many of these cases experimental evidence is lacking. Recently, however, Turing-type structures have been found in the chlorite-iodide-malonic acid reaction [6, 31, 19, 14]. Aside from the difficulty of identifying morphogens and the reactions in which they participate in a biological context, there are several general properties of Turing systems that limit their applicability.

- The spatial patterns in a Turing system typically arise via an instability, and thus the parameters must be tightly controlled to obtain the onset of the instability at the desired point in parameter space. In particular, for a given kinetic mechanism, the diffusion coefficients must have the proper relative magnitudes.
- Because the instabilities result from the interaction of reaction and diffusion, the patterns that arise are sensitive to the overall scale of the system. As a result, it is difficult to obtain the degree of scale-invariance that is observed in various biological systems. However, modifications of Turing’s model can circumvent this difficulty [29, 32].
- Frequently there are multiple stable solutions that coexist in a Turing system (examples are given later), which raises the problem of pattern selection. Generally tight control of the initial conditions is needed to select the desired pattern.

In this paper we analyze the spatial pattern formation properties of a two-component reaction-diffusion system in which the two species are subject to different boundary conditions. For example, one species may be subject to Neumann conditions, whereas the other species may satisfy Dirichlet conditions. We focus our attention on the size of the parameter domain in which multiple solutions are exhibited, the control of the polarity of solutions, and the degree of scale-invariance of solutions.

One of the major points that emerges from our analysis is the following. Fixing one (but not both) species at the boundary leads to less sensitive dependence of patterns on both the length and the initial conditions. In particular, for certain combinations of boundary conditions we find smooth transitions between different spatial patterns, and these transitions do not involve bifurcations. For example, we find a transition from 1 to 2 to 3 stable pattern elements in a one-parameter family

parameterized by the length. Moreover, these solutions are apparently the only stable solutions. By contrast, for Turing systems a tortuous path in parameter space would be required, because different stable patterns may coexist under certain conditions.

In the following section we discuss some general properties of reaction-diffusion systems and describe some of the standard kinetic schemes that are used in pattern formation studies. In particular we point out that the popular terminology that labels certain systems as activator-inhibitor systems is not sufficiently precise: any two-component system that can lead to diffusive instabilities is an activator-inhibitor system. The distinction that should be made is between what we call a pure activator-inhibitor system and a cross activator-inhibitor system. Under conditions to be made precise later, we show that in the former type the gradients of the two species are parallel sufficiently close to a bifurcation point, while in the latter they are anti-parallel (both in one space dimension), and this seems to be the only significant difference between the two types of systems. We then discuss in more detail the parametric behavior of one representative example of a cross activator-inhibitor mechanism.

In Sect. 3 we carry out a qualitative analysis of the solutions for mixed boundary conditions, and analyze the existence and stability of solutions in the limit $L \rightarrow 0$. In Sect. 4 we present some numerical results for various combinations of boundary conditions. The possible application of our results in the context of limb development is discussed in the conclusions section.

2 General results for Turing systems

2.1 The standard Turing model

In the following section we will discuss a specific model reaction mechanism, but here we will simply assume that the temporal dynamics in a spatially uniform system are governed by the solution of the system of differential equations

$$\frac{dc}{dt} = \bar{R}(c, \bar{p}). \quad (1)$$

Here the vector $c = (c_1, c_2, \dots, c_m)$ is the vector of chemical concentrations, and is therefore an element of the nonnegative cone C_m^+ of an m -dimensional real Euclidean vector space. The functions \bar{R}_i give the net rate of production of the i^{th} species and they are usually polynomial or rational functions in the c_i 's, in the latter case having no poles in C_m^+ . The vector \bar{p} is a parameter vector, which can include the kinetic constants and perhaps species that appear in the kinetic mechanism but do not change significantly on the time scale of interest. To be well-posed from the physical standpoint, the solution of (1) should exist and be nonnegative and bounded for $t \in (0, \infty)$. Nonnegativity is guaranteed by the hypothesis that

$$\bar{R}_i(c_1, c_2, \dots, c_{i-1}, 0, \dots, c_m, \bar{p}) \geq 0, \quad (2)$$

for $c_j \geq 0, j \neq i$. The solution through any initial point in C_m^+ will be unique if the functions \bar{R}_i are locally Lipschitz continuous in c throughout C_m^+ .

Let Ω be a bounded region in \mathbb{R}^q , $q \leq 3$ with a smooth boundary and outward normal \mathbf{n} . Turing's model for pattern formation is described by the system of reaction-diffusion equations

$$\begin{aligned} \frac{\partial c}{\partial t} &= D\nabla^2 c + \bar{R}(c, \bar{p}) \quad \text{in } \Omega \\ \mathbf{n} \cdot D\nabla c &= H(c^* - c) \quad \text{on } \partial\Omega \\ c(r, 0) &= c_0(r), \end{aligned} \tag{3}$$

where c^* is a fixed concentration and D is usually assumed to be a constant diagonal matrix. We assume for the present that all $D_i > 0$. The matrix H of mass transfer coefficients is also diagonal, and when $H_i = \infty$ one has Dirichlet data on the i^{th} species, whereas if $H_i = 0$ one has Neumann data.

Let ω^{-1} be a time scale characteristic of the reactions, let L be a measure of the size of the system, and let C_i be a reference concentration for the i^{th} species. Suppose that the species are ordered so that $\max_i \{D_i\} = D_1$. Define the dimensionless quantities $u_i = c_i/C_i$, $\tau = \omega t$, $\delta^i = D_i/D_1$, $v = D_1/\omega L^2$, and $\zeta = r/L$, where $r \equiv (x_1, \dots, x_q)$. The dimensionless governing equations are

$$\begin{aligned} \frac{\partial u}{\partial \tau} &= v\mathcal{D}\nabla^2 u + R(u, p) \quad \text{in } \Omega \\ \mathbf{n} \cdot \nabla u &= P(u^* - u) \quad \text{on } \partial\Omega \\ u(\zeta, 0) &= u_0(\zeta), \end{aligned} \tag{4}$$

where $\mathcal{D} = \text{diag}\{1, \delta^2, \dots, \delta^m\}$, $P_i = LH_i/D_i$, and $R(u, p)$ is the dimensionless form of $\bar{R}(u, p)$.

Proposition 1 of Ashkenazi and Othmer [1] shows that for most of the typical rate laws used, the condition (2) that guarantees invariance of C_m^+ under the flow of (1) also guarantees that classical solutions of the reaction-diffusion system (4) will be nonnegative for $t > 0$ provided that the initial data is nonnegative. Furthermore, these authors show that the solution of (4) exists and is unique for sufficiently small times and that the solution is bounded in $L_1(\Omega)$ for $t \in [0, \infty)$ under minimal smoothness conditions on the vectorfield. If the kinetic vectorfield admits an invariant rectangle then one can also show that the solution exists for all time pointwise in space [8]. Thus the models we use are well-posed from a physical standpoint (as well as being well-posed in the standard mathematical sense).

In the absence of reaction, the solution relaxes exponentially to the average concentration set by the initial conditions under Neumann boundary conditions. Thus one expects that a system will relax to a uniform state whenever the relaxation time for diffusion of each species is sufficiently short compared to that of the chemical reactions. The dimensionless quantity $\omega^{-1}/(L^2/D_i)$ is the ratio of a kinetic relaxation time to a relaxation time for diffusion, and thus one expects that when L is small enough the system will relax to a uniform state if all $D_i > 0$. This can be shown rigorously using a theorem in [24]. An order of magnitude estimate given there shows that for typical values of the diffusion coefficients and kinetic relaxation times it can be expected that systems of order two cell diameters in size will relax to a uniform state provided that all time-dependent species involved in the kinetic terms also diffuse. A similar result holds for the Dirichlet problem provided that u^* is such that $R(u^*, p) = 0$ [8]. However, Turing showed

that diffusion could destabilize a steady state that is stable in the absence of diffusion, and when this occurs one calls it a diffusive instability. In order to define this precisely, we have to consider the variational system associated with (4).

Suppose that u^s is a time-independent solution of (4). If we linearize (4) around u^s and let $\xi = u - u^s$, then we obtain the variational system

$$\begin{aligned} \frac{\partial \xi}{\partial \tau} &= v\mathcal{D}\nabla^2 \xi + K\xi \\ \mathbf{n} \cdot \nabla \xi &= -P\xi \\ \xi(\zeta, 0) &= \xi_0(\zeta), \end{aligned} \tag{5}$$

where

$$K \equiv \begin{bmatrix} k_{11} & \dots & k_{1m} \\ \vdots & & \vdots \end{bmatrix},$$

and $k_{ij} = \partial R_i / \partial u_j(u^s)(\zeta)$. This system has solutions of the form $\xi = e^{\lambda\tau}\Psi$, which leads to the spectral problem

$$\begin{aligned} v\mathcal{D}\nabla^2\Psi + (K - \lambda I)\Psi &= 0 \\ \mathbf{n} \cdot \nabla\Psi &= -P\Psi. \end{aligned} \tag{6}$$

This is generally not a self-adjoint problem, and the eigenfunctions do not have a simple form, even if u^s is independent of ζ . Suppose however, that $P = \rho I$ for some $\rho \in \mathfrak{R}^+$, in which case we say that the boundary conditions are scalar conditions.¹ If in addition u^s is a constant, then the eigenfunctions can be written $\Psi_{jn} = y_{jn}\phi_n$, where ϕ_n is a solution of the scalar eigenvalue problem

$$\begin{aligned} \nabla^2\phi_n &= -\alpha_n^2\phi_n \text{ in } \Omega \\ \mathbf{n} \cdot \nabla\phi_n &= -\rho\phi_n \text{ on } \partial\Omega. \end{aligned} \tag{7}$$

The vector $y_{jn} \in \mathfrak{R}^m$ is a solution of the algebraic eigenvalue problem

$$(K - \mu_n\mathcal{D} - \lambda I)y = 0, \tag{8}$$

where $\mu_n \equiv \alpha_n^2 v$. In this case the eigenfunctions are complete and the solution of the linear variational problem can be written

$$\xi(\zeta, \tau) = \sum_{n=0}^{\infty} e^{(K - \mu_n\mathcal{D})\tau} y_n \phi_n(\zeta) \tag{9}$$

where the $y_n \in \mathfrak{R}^m$ are determined by the initial data. This case is particularly simple, because the eigenfunctions of the variational problem are independent of the parameter L , and one can characterize the solution of the full nonlinear problem by specifying its amplitude spectrum relative to a basis comprised of those eigenfunctions. When the underlying solution u^s is not constant the eigenfunctions vary with L . If the eigenfunctions are complete one can still characterize the solutions by their amplitude spectrum relative to the eigenfunction basis, but this

¹ In fact, we can allow the possibility that $\partial\Omega$ has several connected components, on each of which the boundary condition is scalar, with a different ρ for each component of the boundary

cannot be done uniformly in L . However, one can still characterize solutions in terms of the number of maxima or minima, and this is adequate if it is only the threshold levels of morphogens that are important. For some purposes it is appropriate to use a fixed basis, such as trigonometric functions, for the solution of the variational problem, and this is done for the linear analysis in Appendix A.

The foregoing shows that stability in an $L_2(\Omega)$ sense for the linear equations with scalar boundary conditions is governed by the eigenvalues of the family $\{K - \mu_n \mathcal{D}\}_{n=0}^\infty$, and it is well-known that the principle of linearized stability holds for equations like (5). That is, asymptotic stability or instability for the zero solution of the variational equations implies the same properties of the solution u^s of the nonlinear equations. The spatial variation of any mode is given by $\phi_n(\zeta)$, but in the case $\rho = 0$ ($\rho = \infty$) this can be written

$$\phi_n(\zeta) = \phi(\alpha_n \zeta) = \phi\left(\frac{\alpha_n}{L} r\right), \tag{10}$$

where ϕ solves the problem

$$\nabla^2 \phi = -\phi \quad \text{in } \Omega$$

with homogeneous Neumann (homogeneous Dirichlet) boundary conditions. That is, by scaling ζ by α_n we obtain a universal pattern function, and the eigenfunctions differ from each other only by the dilation α_n/L of the spatial scale. Thus homogeneous Dirichlet and Neumann boundary conditions play a distinguished role in the context of Turing instabilities.

Although $\{\mu_n\}$ is countable for a reasonable domain, it is convenient at present to replace μ_n with a continuous variable. Then stability of u^s is governed by the character of the eigenvalues of the one-parameter family of matrices $\{K - \mu \mathcal{D}\}$ for $\mu \in \mathfrak{R}^+$, and a diffusive instability is defined as follows.

Definition 1 Suppose that u^s is asymptotically stable as a steady-state solution of (1). We say that a *zero-amplitude diffusive instability* of u_1^s exists if there exist μ^\pm , $0 < \mu^- \leq \mu^+ < \infty$, such that $K - \mu \mathcal{D}$ has at least one eigenvalue with a positive real part when $\mu \in (\mu^-, \mu^+)$. If for some $\mu^* \in (\mu^-, \mu^+)$, $K - \mu^* \mathcal{D}$ has a single real positive eigenvalue the instability is *stationary* at μ^* , while if $K - \mu^* \mathcal{D}$ has complex eigenvalues with a positive real part the instability is *oscillatory* at μ^* .

Of course it is possible that $K - \mu \mathcal{D}$ has real positive eigenvalues and complex eigenvalues with a positive real part at some μ^* , or there may be several disjoint intervals of μ in which $K - \mu \mathcal{D}$ has an eigenvalue with a positive real part. Usually one is only interested in knowing whether the first eigenvalue to cross from the left-half to the right-half plane is real or complex, and for this the above characterization suffices when the eigenvalue having the largest real part is simple. Stationary instabilities generically lead to bifurcation of a stationary solution from u^s , whereas oscillatory instabilities generically lead to bifurcation of periodic solutions from u^s .

Let K^s denote the symmetric part of K , let $\sigma(K)$ denote the spectrum of the matrix K , let LHP (LHP) denote the open (closed) left-half complex plane, and let $\|\cdot\|$ denote the Euclidean norm in R^n . Some general conditions on K and \mathcal{D} that preclude diffusive instabilities are given in the following theorem. In this theorem

and the one that follows there is no reference to the type of boundary conditions imposed, but it is assumed that the boundary conditions are scalar conditions.

Theorem 2 [27] *Suppose that \mathcal{D} is diagonal with $\mathcal{D}_i \geq 0$. Then each of the following conditions is sufficient to preclude diffusive instabilities.*

- *K and \mathcal{D} are simultaneously triangularizable.*
- *There exists a diagonal matrix W with $W_i > 0$ such that $\sigma(WK)^s \subset LHP$.*
- *K is either row or column quasi-diagonally dominant.*
- *$\min_i \mathcal{D}_i / \max_i \mathcal{D}_i > 1 - 1/m$, where m is such that $\| \exp(Kt) \| \leq m \exp(-\gamma t)$, and $m \geq 1, \gamma > 0$.*
- *The graph $\mathcal{G}(K)$ associated with K has no cycles of length greater than one.*

However, it is also well known that a diffusive instability is possible given the proper structure in the kinetic mechanism. The following theorem summarizes the necessary conditions for stability, and from this one can understand the type of kinetic interactions that can give rise to diffusive instabilities. In the theorem, $K[i_1, i_2, \dots, i_p]$ denotes a $p \times p$ principal submatrix of K formed from rows and columns i_1, i_2, \dots, i_p for $1 \leq p \leq n - 1$.

Theorem 3 [26] *Let \mathcal{D} be diagonal with $\mathcal{D}_j \geq 0$. In order that $\sigma(K - \mu\mathcal{D}) \subset LHP$ for all such \mathcal{D} and all $\mu \in [0, \infty)$, it is necessary that*

- *$\sigma(K) \subset LHP$*
- *$\sigma(K[i_1, i_2, \dots, i_p]) \subset \overline{LHP}$ for all p^{th} -order submatrices of K , where $1 \leq p \leq n - 1$.*

It is clear that scalar boundary conditions greatly simplify the linear analysis, for the eigenfunctions have a simple product form. Thus far little is known about (6) when the boundary conditions are not scalar conditions. General results on selected types of mixed conditions would be useful for understanding pattern formation in biological systems that have mixed conditions.

2.2 Diffusive instabilities in a two-component Turing model

Since we later restrict attention to two-species systems, we shall briefly review some of the known facts about such systems; for further details and generalizations see [23, 30, 24, 29, 22]. To simplify the notation, we let (u, v) denote the chemical species, we denote the reaction vector field by $(f(u, v, p), g(u, v, p))$, and we set $\delta_2 = \delta$. We write the governing equations as

$$\begin{aligned}
 \frac{\partial u}{\partial \tau} &= v \nabla^2 u + f(u, v, p) \\
 \frac{\partial v}{\partial \tau} &= \delta v \nabla^2 v + g(u, v, p)
 \end{aligned}
 \qquad \text{in } \Omega$$

$$\begin{aligned}
 \mathbf{n} \cdot \nabla u &= \rho(u^* - u) \\
 \mathbf{n} \cdot \nabla v &= \rho(v^* - v).
 \end{aligned}
 \qquad \text{on } \partial\Omega$$
(11)

Then the stability of (u^s, v^s) is governed by the character of the eigenvalues of the problem

$$\det(K - \mu\mathcal{D} - \lambda I) = \lambda^2 + c_1(\mu)\lambda + c_2(\mu) = 0.$$
(12)

Here

$$\begin{aligned}
 c_1(\mu) &\equiv \mu \operatorname{trace} \mathcal{D} - \operatorname{trace} K = \mu(1 + \delta) - (k_{11} + k_{22}) \\
 c_2(\mu) &\equiv \mu^2 \det \mathcal{D} + \mu(\operatorname{trace}(K\mathcal{D}) - (\operatorname{trace} K)(\operatorname{trace} \mathcal{D})) + \det K \\
 &= \mu^2 \delta - \mu(k_{11} \delta + k_{22}) + \det K,
 \end{aligned}
 \tag{13}$$

and $\operatorname{trace} A$ ($\det A$) stand for the trace and determinant, respectively, of any matrix A . One is usually interested in how the eigenvalues change as some parameter p is varied, and in particular, in whether or not a diffusive instability is possible.

The solution (u^s, v^s) is asymptotically stable as a solution of (1) if $\operatorname{trace} K < 0$ and $\det K > 0$, and we assume that these conditions hold hereafter. Furthermore, it follows from the definition of $c_1(\mu)$ that if $c_1(0) > 0$, then an oscillatory diffusive instability is impossible provided that the diffusion coefficients are nonnegative. Only stationary diffusive instabilities can occur for $D_i \geq 0$, and it follows from (8) that under the standing conditions on K , $c_2(\mu)$ can vanish only if $k_{ii} > 0$ for $i = 1$ or 2 . Without loss of generality we can assume that $k_{22} > 0$, and then it is necessary that $k_{11} < 0$ and that $k_{12}k_{21} < 0$ in order that $\operatorname{trace} K < 0$ and $\det K > 0$. The range of dimensionless wave numbers in which $c_2(\mu) < 0$ is (μ^-, μ^+) , where

$$\mu^\pm = (k_{22} + \delta k_{11} \pm \sqrt{(k_{22} + \delta k_{11})^2 - 4\delta \det K})/2\delta,
 \tag{14}$$

and in this interval $K - \mu\mathcal{D}$ has exactly one real positive eigenvalue. In order that μ be ≥ 0 , it is necessary that $\delta \leq 1$, and since $\operatorname{trace} K < 0$, there can never be two real positive eigenvalues.

Within an arbitrary relabelling of species, any two-component kinetic mechanism that can lead to a diffusive instability must give rise to a Jacobian at (u^s, v^s) with one of the following patterns of signs.

$$K_p \equiv \begin{bmatrix} - & + \\ - & + \end{bmatrix} \quad K_c \equiv \begin{bmatrix} - & - \\ + & + \end{bmatrix},
 \tag{15}$$

Definition 4 A kinetic mechanism for which the Jacobian at $u \in \bar{C}_2^+$ is of type K_p (type K_c) is said to be a *pure (cross) activator-inhibitor mechanism* at u .

Clearly the type of a mechanism may vary with $u \in \bar{C}_2^+$, but when it does not we call the mechanism a *global pure (cross) activator-inhibitor system*. Comparison theorems can be used to prove existence of the solution of (11) for all time for mechanisms whose type is global. In studying zero-amplitude diffusive instabilities the interest is in the local behavior near a steady state, and Fig. 1 shows the only possibility for the local disposition of the isoclines $f = 0$ and $g = 0$ for each of the two types. As shown there, for a pure activator-inhibitor system the level sets $f = 0$ and $g = 0$ must lie in the first and third quadrants sufficiently close to the origin in a coordinate system centered at (u^s, v^s) , whereas they must lie in the second and fourth quadrants for a cross activator-inhibitor system.

Currently the terminology ‘activator-inhibitor’ is primarily used to describe a global pure activator-inhibitor mechanism [20]. However it is clear (and well known) that any two-component system that leads to a zero-amplitude diffusive instability must contain both self-activation and mutual or cross activation and inhibition. The distinction between the two generic types hinges on whether the self-activating species activates or inhibits the other species. The major qualitative

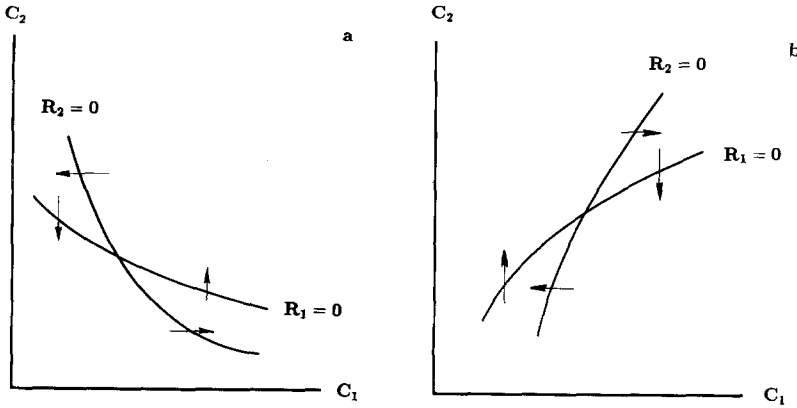


Fig. 1.a, b A schematic of the local behavior of the nullclines for the two generic types of two-component systems that support diffusive instabilities. a a cross activator-inhibitor system, b a pure activator-inhibitor system

difference in the concentration profiles for the two types of mechanism under homogenous Neumann conditions is stated in the following proposition.

Proposition 5 *Suppose that $\rho = 0$ in (11). If the kinetic mechanism is of global pure (cross) type and $q = 1$, then non-constant solutions that bifurcate from the uniform steady state have the property that $\text{sgn}(u_\zeta) = \text{sgn}(v_\zeta)$ ($\text{sgn}(u_\zeta) = -\text{sgn}(v_\zeta)$) in some neighborhood of the bifurcation point. In other words, the gradients are locally antiparallel (parallel).*

Proof. By differentiating the one-dimensional, time-independent version of (11) one finds that

$$v(u_\zeta)_{\zeta\zeta} + f_u u_\zeta + f_v v_\zeta = 0 \tag{16}$$

$$\delta v(v_\zeta)_{\zeta\zeta} + g_u u_\zeta + g_v v_\zeta = 0. \tag{17}$$

It suffices to prove the result for either of the cases, for if one is proved the other follows after the transformation $v_\zeta \mapsto -v_\zeta$. The conclusion is easily established near a bifurcation point on the uniform steady state, whether or not the corresponding eigenvalue is simple. This is done by solving the system at the bifurcation point, where it has constant coefficients, and then applying a perturbation argument.

As we shall see later, the numerical results suggest that the conclusion is true on all primary bifurcating branches, not only near the bifurcation point, but it is not true on the secondary bifurcating branches. This result implies that to a first approximation, the only admissible phase differences between the two species are 0 and π in a one-dimensional system.

Next we analyze in more detail how the intervals of unstable wave numbers depend on the linearized kinetic parameters and on the ratio of diffusion coefficients. It follows from the definition of $c_2(\mu)$ that $\mu^\pm > 0$ only if $\delta < -k_{22}/k_{11}$.

Furthermore, for fixed k_{ij} the discriminant of (13) is a quadratic in δ , the roots of which are

$$\delta^\pm = \frac{\det K - k_{12}k_{21} \pm 2\sqrt{-k_{12}k_{21} \det K}}{k_{11}^2}.$$

It can be shown that

$$0 < \delta^- < \frac{-k_{22}}{k_{11}} < \delta^+,$$

and therefore the maximum allowable δ for which a zero-amplitude diffusive instability occurs at some $\mu > 0$ is $\delta^c \equiv \delta^-$. Note that if trace $K = \det K = 0$, then $\delta^\pm \rightarrow 1$, which means that a diffusive instability can occur when the ratio of the diffusion coefficients is arbitrarily close to one, provided that both eigenvalues of the Jacobian for the kinetics are sufficiently close to zero. This conclusion carries over to n -component systems as well [33].

At the critical value of δ

$$\mu^+ = \mu^- \equiv \mu^c = \frac{k_{22} + \delta^c k_{11}}{2\delta^c}. \tag{18}$$

The corresponding critical wave number is

$$\frac{\alpha^c}{L} \equiv \sqrt{\frac{\mu^c \omega}{D_1}} = \sqrt{\frac{\omega}{D_1} \left(\frac{k_{22} + \delta^c k_{11}}{2\delta^c} \right)}. \tag{19}$$

This is a natural or intrinsic wavelength at marginal instability, which Turing [34] called the chemical wavelength. In a one-dimensional system of length L with homogeneous Neumann boundary conditions, $\alpha_n = n\pi, n = 0, 1, \dots$ and $\phi_n = \cos(n\pi/L)\zeta$, while under homogeneous Dirichlet conditions $\alpha_n = n\pi, n = 1, \dots$ and $\phi_n = \sin(n\pi/L)\zeta$. In either case the critical wave number is indexed by the integer n closest to [29]

$$\frac{L}{\pi} \sqrt{\frac{\omega}{D_1} \left(\frac{k_{22} + \delta^c k_{11}}{2\delta^c} \right)}.$$

If the entries of K and \mathcal{D} are such that there is a positive real eigenvalue of $K - \mu\mathcal{D}$ for $\mu \in [\mu^-, \mu^+]$, then the mode ϕ_n is unstable whenever

$$L \in [L_n^-, L_n^+] = \left[n\pi \sqrt{\frac{D_1}{\omega\mu^+}}, n\pi \sqrt{\frac{D_1}{\omega\mu^-}} \right]. \tag{20}$$

Thus the intervals of instability of the successive modes are disjoint if and only if

$$\frac{n-1}{n} < \sqrt{\frac{\mu^-}{\mu^+}}$$

i.e., if and only if

$$n < n^* \equiv \frac{1}{1 - \sqrt{\frac{\mu^-}{\mu^+}}}.$$

As L increases from zero the uniform steady state always loses stability with respect to ϕ_1 first and is linearly unstable with respect to ϕ_1 over the range

$$\Delta L_1 \equiv L_1^+ - L_1^- = \pi \sqrt{\frac{D_1}{\omega}} \left[\frac{1}{\sqrt{\mu^-}} - \frac{1}{\sqrt{\mu^+}} \right].$$

The foregoing results can also be applied to systems with scalar boundary conditions of the third type (i.e., when $\rho \neq 0$), and to arbitrary domains. In the former case one simply replaces $n\pi$ by α_n in (20). In the latter case one regards L as some measure of the size of the system, and one replaces $n\pi$ by the n^{th} eigenvalue of the Laplacian for the domain in question in (20). Of course real two- or three-dimensional growth can rarely be described by a single size parameter since proportions usually change during growth. The same sort of analysis that was done for two-component systems can be done for n -component systems as well, although the critical quantities cannot be computed explicitly in general [23, 30]. Furthermore, when $n \geq 3$ there may be more than one turning point on the curve $\det(K - \mu \mathcal{D})$ in the μ versus δ^i plane.

A simple measure of the range of invariance of pattern formation in Turing's model with scalar homogeneous Neumann or Dirichlet conditions is the interval of instability for the n^{th} mode, which is given by

$$\Delta L_n = n\pi \sqrt{\frac{D_1}{\omega}} \left[\frac{1}{\sqrt{\mu^-}} - \frac{1}{\sqrt{\mu^+}} \right].$$

This criterion is similar to the one used in [18]. Clearly it depends on the mode number in question. Furthermore, when the intervals overlap, as they always do for large enough n or sufficiently small δ , the uniform state is unstable with respect to more than one mode and it is possible that more than one solution is stable or that the spatial distribution of the morphogens in the stable solution bears little resemblance to the spatial variation of the eigenfunctions. Thus the foregoing linear analysis gives little information about scale-invariance in the full nonlinear model in these cases. However, one can certainly conclude already that Turing's model does not show perfect scale-invariance (a conclusion reached by others [29, 32, 2, 17] and one that does not rest on any of the foregoing analysis). It is of course very difficult to say anything analytically about the behavior of the solutions of the full nonlinear equations, except near certain degenerate points corresponding to coincidence of an L_j^+ and an L_k^- (cf. Fig. 4b). However some insight into the changes in the spatial distributions that must occur as the parameter L varies can be gotten as follows. Time-independent solutions of (4) exist when the diffusion rate is balanced by the reaction rate at each point in space. As L increases the relaxation time for diffusion increases and at least one of three possible changes in the profiles must occur. Firstly, the local curvature of the distributions could increase so as to maintain a constant diffusion rate. Secondly, the local diffusion rate could decrease and the reaction rate could change correspondingly. Finally, the local amplitude of the solution could increase, again so as to maintain the diffusion rate constant. The last of these is only possible if the reaction rates are insensitive to changes in concentration, which can occur for enzymatic reactions only when the rate is saturated at maximal velocity. Of course a combination of the foregoing changes is generally what occurs, but under any of them the spatial profile varies with L and in particular, the spatial location of fixed

concentration thresholds that are used to trigger differentiation into different types of cells will generally move about in space. The precise amount of this drift can only be determined on a case-by-case basis, but some general conclusions can be derived from studies of model systems. In the following sections we study the effect of nonscalar boundary conditions on the intervals of instability and on the types of stable patterns that can arise.

3 Systems with mixed boundary conditions

3.1 Qualitative analysis

We saw in the previous section how the intervals of instability for a linear Turing system depend on the parameters, and in particular, we determined when these intervals overlap as a function of the length. When the intervals are disjoint a single real eigenvalue crosses the imaginary axis at L_n^- , and the uniform steady state becomes unstable to a spatial pattern given by $\phi(\zeta)$ (cf. (10)). In general, a nonconstant solution bifurcates at L_n under a nondegeneracy condition on the nonlinearity (specific examples are given later). These conclusions hold in any number of spatial dimensions, but hereafter we restrict attention to one-dimensional systems. For Neumann boundary conditions the spatial variation of the unstable mode is $\phi_n = \cos((n\pi/L)x)$. As we observed earlier, in the linear approximation the spatial phase difference between the two components is either 0° or 180° , according as the mechanism is locally of pure or cross activator-inhibitor type. This phase relationship is not precisely preserved in the solution of the full nonlinear problem, but results from bifurcation theory show that spatial variation of the solution near the bifurcation point is dominated by the unstable eigenfunction near the bifurcation point, and numerical results given later show that the phase relations do not change significantly, even far from the bifurcation point.

To gain some insight into the effects on time-independent spatial patterns of changing the boundary conditions, we will consider different combinations of Neumann and Dirichlet conditions on the two components. In the following analysis we only consider the cases in which $(u^*, v^*) = (0, 0)$ and $(u^*, v^*) = (u^s, v^s)$, but in the next section we allow a more general nonhomogeneous term. The steady state equations are

$$\begin{aligned}vu_{\zeta\zeta} + f(u, v, p) &= 0 \\ \delta v v_{\zeta\zeta} + g(u, v, p) &= 0\end{aligned} \quad \text{in } (0, 1) \tag{21}$$

The boundary conditions will be written in the form

$$\begin{aligned}\theta_1 \frac{\partial u}{\partial n} &= \rho(1 - \theta_1)(\theta_3 u^s - u) \\ \delta\theta_2 \frac{\partial v}{\partial n} &= \delta\rho(1 - \theta_2)(\theta_3 v^s - v),\end{aligned} \quad \text{for } \zeta = 0, 1 \tag{22}$$

where $\theta_i \in [0, 1]$, $i = 1, 2, 3$, are homotopy parameters. Our strategy in the numerical computations described in the following section will be to do a homotopy between various types of boundary conditions by varying the parameters θ_i . To facilitate reference to various limiting cases of the homotopies, we first introduce some terminology.

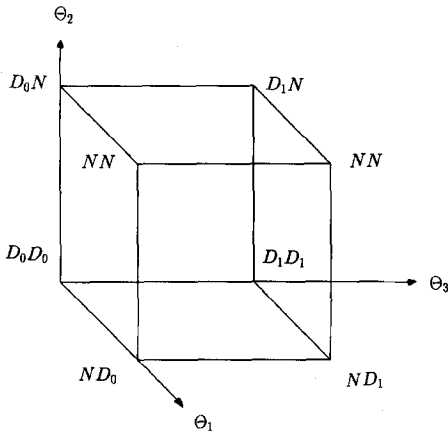


Fig. 2. A schematic showing the relationship of various combinations of boundary conditions to the homotopy parameters

When $(\theta_1, \theta_2, \theta_3) = (1, 1, \cdot)$ the governing Eqs. (21) and (22) reduce to the pure homogeneous Neumann problem, which we denote NN . If $(\theta_1, \theta_2, \theta_3) = (1, 0, 0)$, then the problem has a homogeneous Neumann condition on u and a homogeneous Dirichlet condition on v . We denote this case by ND_0 . If $(\theta_1, \theta_2, \theta_3) = (0, 1, 0)$ we have the mixed boundary problem D_0N , and if $(\theta_1, \theta_2, \theta_3) = (0, 0, 0)$ we have the pure homogeneous Dirichlet problem D_0D_0 . Similarly, if we fix $(\theta_1, \theta_2, \theta_3) = (1, 0, 1)$ then (21) and (22) reduce to the mixed boundary problem with a homogeneous Neumann condition on u and a nonhomogeneous Dirichlet condition on v , denoted ND_1 . Finally, for $(\theta_1, \theta_2, \theta_3) = (0, 1, 1)$ we have the mixed boundary problem D_1N , while for $(\theta_1, \theta_2, \theta_3) = (0, 0, 1)$ we have the pure nonhomogeneous Dirichlet problem D_1D_1 . Figure 2 illustrates the relationship between the various problems. We will expand on this figure later to summarize how the solutions change as various edges are traversed.

Equation (21) defines a dynamical system in \mathfrak{R}^4 , and the solution of (21) subject to (22) defines a curve $\tilde{\Gamma}: [0, 1] \rightarrow C_2^+ \times \mathfrak{R}^2$. In the case D_1D_1 the endpoints of $\tilde{\Gamma}$ lie in the two-dimensional manifold $(u^s, v^s) \times \mathfrak{R}^2$, while in the case NN the endpoints lie in $C_2^+ \times (0, 0)$. The projection of $\tilde{\Gamma}$ into \mathfrak{R}^2 shows how the gradients vary along the solution, and the projection of $\tilde{\Gamma}$ into C_2^+ , which we call Γ , reflects the variation of (u, v) . For example, consider the case NN . By integrating both equations in (21) over $[0, 1]$ we find that

$$\int_0^1 f(u, v, p) d\zeta = 0 \tag{23}$$

and

$$\int_0^1 g(u, v, p) d\zeta = 0. \tag{24}$$

Thus the average reaction rate must vanish. In the case ND_i and D_iN , for $i = 0, 1$, the corresponding average rate must still vanish for the species that satisfies a Neumann condition, irrespective of the boundary condition imposed on the other species. To see how these elementary facts enable us to get some insight into the behavior of the curve Γ as the boundary conditions are changed, we must consider a specific reaction mechanism. In the previous section we showed that there are only two generic types of two-component systems when viewed in the linear

approximation, and in the remainder of the paper we focus on one of these. We consider a simplified version of a model for glycolysis, which is obtained from the general model in the limiting case in which the enzymes are far from saturation [28, 1].

The vectorfield is

$$\begin{aligned} f(u, v, p) &= \beta - \kappa u - uv^2 \\ g(u, v, p) &= \kappa u + uv^2 - v, \end{aligned} \tag{25}$$

where β and κ are parameters that we set to 1.0 and 0.001, respectively. A sketch of the nullclines for this mechanism is shown in Fig. 3.² This system is a cross activator-inhibitor mechanism whenever $2uv > 1$, and in particular, this is true at the steady state whenever $\beta^2 > \kappa$. For these values of β and κ , $\delta_c \sim 0.172$, and μ^\pm are as shown in Fig. 4a. If we also choose $D_1 = 10^{-5}$ cm²/sec and $\omega = 0.01$ sec⁻¹, then we can compute the range of unstable lengths for the various modes. The results for the first four modes are shown as a function of δ in Fig. 4b (cf. also Table 1). Figures 4a, b both apply to homogeneous Neumann conditions and to homogeneous Dirichlet conditions.

To see how the boundary conditions affect Γ , we sketch the possibilities as $(\theta_1, \theta_2, \theta_3)$ varies using the glycolytic vectorfield. When $(\theta_1, \theta_2, \theta_3) = (1, 1, \cdot)$, the location of Γ is constrained only by the integral conditions given by (23) and (24), which imply that Γ cannot lie entirely on one side of either $f = 0$ or $g = 0$. One feasible curve is shown in Fig. 5a.

When $(\theta_1, \theta_2, \theta_3) = (1, 0, 0)$ (case ND_0), Γ must cross $f = 0$ at least once, and it must terminate on the u -axis. One possibility that satisfies these conditions is

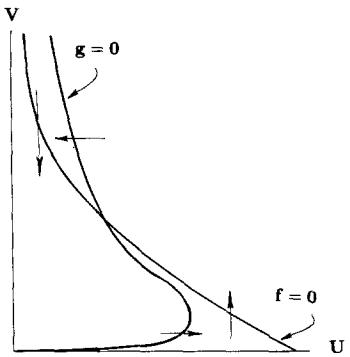


Fig. 3. The nullclines for the model of glycolysis

² It is easy to see that there is no invariant rectangle in C_2^+ for the flow in \mathbb{R}^2 defined by (1) when \bar{R} is given by (25). Therefore one cannot assert a priori that all solutions of the reaction-diffusion system are bounded. In fact, one can see from Fig. 3 that $g > 0$ for fixed u sufficiently large, and large v , and this suggests that there may be solutions for which v is unbounded. However, this is an artifact that arises from the simplification of the original model. If the positive feedback term uv^2 is replaced by a function such as $\gamma uv^2/(K + v^2)$ that saturates at large v , then it is easy to show that the local dynamics has an invariant rectangle, and that all solutions of the reaction-diffusion system are bounded. Our interest here is in solutions of moderate amplitude, and solutions of (21) and (22) are small perturbations of the solutions of the more complete equations in this range. Therefore whether or not there are also large-amplitude solutions is irrelevant for our purposes

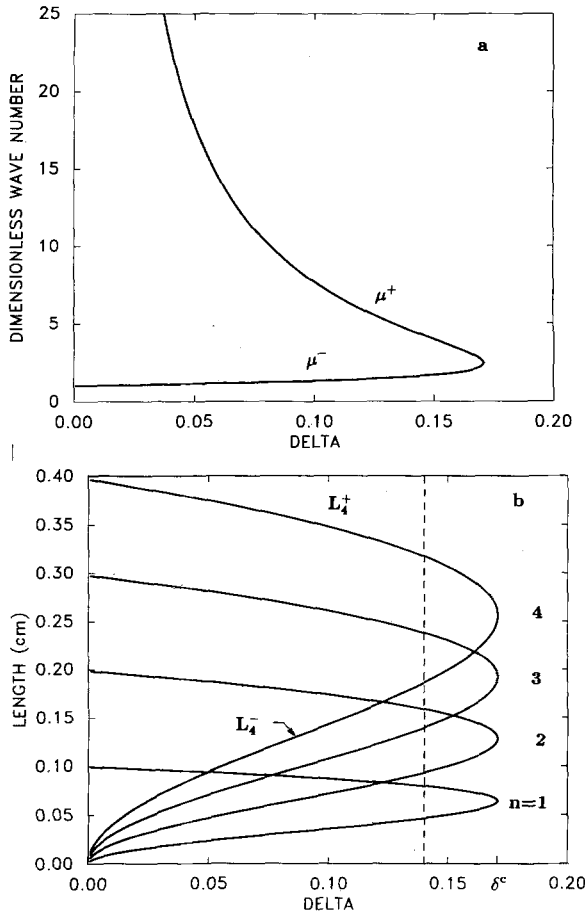


Fig. 4. **a** The locus of marginal stability for the glycolytic reactions in δ - wave number space. **b** The intervals of instability for the first four modes in δ -L space

Table 1. Numerical and analytical values of the endpoints of the instability intervals $[L_i^-, L_i^+]$ (in cm) for the i^{th} mode in case NN . The analytic values are obtained using (20); the numerical procedures will be discussed in the following section

NN	L_1^-	L_1^+	L_2^-	L_2^+	L_3^-	L_3^+	L_4^-	L_4^+	L_5^-
Computed	0.047	0.080	0.093	0.159	0.140	0.238	0.186	0.317	0.232
Analytic	0.0465	0.0793	0.093	0.159	0.140	0.238	0.186	0.317	0.233

shown in Fig. 5b. Since $g > 0$ when $v = 0$, $v_{\zeta\zeta} < 0$ near 0 and 1. If Γ crosses $f = 0$ an odd number of times there are an odd number of inflection points in the graph of $u(\zeta)$, and $\text{sgn}(u_\zeta)$ must be the same near 0 and 1. It follows that $\text{sgn}(u_\zeta) = \text{sgn}(v_\zeta)$ in some interval in $[0, 1]$, even for this cross activator-inhibitor system. This is in contrast with the case of Neumann data. When $(\theta_1, \theta_2, \theta_3) = (0, 1, 0)$ (case D_0N), there are several possibilities for the disposition of Γ , as shown in Fig. 5c. In particular, one sees that there are two distinct possibilities as $L \rightarrow 0$, one in which both u and v approach zero throughout $[0, 1]$, and another in which u tends to zero

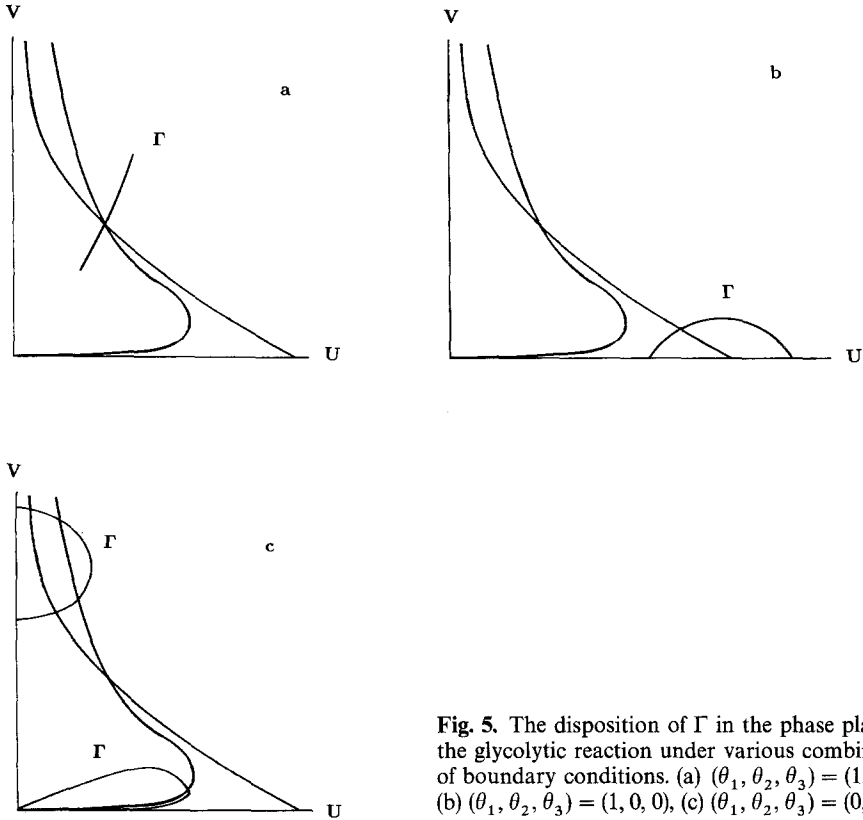


Fig. 5. The disposition of Γ in the phase plane for the glycolytic reaction under various combinations of boundary conditions. (a) $(\theta_1, \theta_2, \theta_3) = (1, 1, \cdot)$, (b) $(\theta_1, \theta_2, \theta_3) = (1, 0, 0)$, (c) $(\theta_1, \theta_2, \theta_3) = (0, 1, 0)$

but v tends to infinity. (As we remarked earlier, the latter possibility is of no interest.) The sketches for the cases D_1N and ND_1 can be gotten from (b) (respectively, (c)) by translating Γ to the line $u = u^s$ (respectively, $v = v^s$).

3.2 Existence and stability for small L

As we observed in Sect. 2, in cases NN and D_1D_1 all solutions converge to a spatially-uniform solution at sufficiently small L . However, this is not true in general for mixed boundary conditions, as we now show. We first establish the existence of solutions at small L , and then we analyze their stability. In the cases ND_1 and D_1N there is a spatially-uniform steady state solution. This is not true in the cases ND_0 , D_0N and D_0D_0 .

First consider the cases ND_i , with i equal to zero or one. Recall that $v \equiv D_1/\omega L^2$ and let $\varepsilon^2 \equiv v^{-1}$. Equations (21) and (22) then become

$$\begin{aligned}
 u_{\zeta\zeta} + \varepsilon^2 f(u, v, p) &= 0 \\
 \delta v_{\zeta\zeta} + \varepsilon^2 g(u, v, p) &= 0,
 \end{aligned}
 \quad \text{in } (0, 1) \tag{26}$$

and

$$\begin{aligned} \frac{\partial u}{\partial \zeta} \Big|_{0,1} &= 0 \\ v|_{0,1} &= c_0, \end{aligned} \tag{27}$$

where c_0 is either zero or v^s . As $L \rightarrow 0, \varepsilon \rightarrow 0$, and for classical solutions this is a regular perturbation problem. Thus we may assume solutions of the form

$$\begin{aligned} u &= u_0 + \varepsilon^2 u_1 + \dots \\ v &= v_0 + \varepsilon^2 v_1 + \dots \end{aligned} \tag{28}$$

At lowest order one finds that $u_0(\zeta) = c_1, v_0(\zeta) = c_0$, where c_1 is to be determined. The solvability condition at $\mathcal{O}(\varepsilon^2)$ reduces to the condition that $f(u_0, v_0, p) = 0$, which yields c_1 , and the components at order $\mathcal{O}(\varepsilon^2)$ are

$$\begin{aligned} u_1 &= c_2 \\ v_1 &= \frac{g(u_0, v_0, p)}{2\delta} (\zeta - \zeta^2) \end{aligned} \tag{29}$$

where c_2 is a constant. The solvability condition at $\mathcal{O}(\varepsilon^4)$ implies that

$$c_2 = - \frac{f_v(u_0, v_0, p)}{f_u(u_0, v_0, p)} \int_0^1 v_1(\zeta) d\zeta. \tag{30}$$

One finds that at $\mathcal{O}(\varepsilon^4)$ the u component of the solution has nontrivial dependence on ζ .

It follows that as $L \rightarrow 0$ the solution converges to $(u, v) = (f^{-1}(0), 0)$ if $c_0 = 0$ (case ND_0), while if $c_0 = v^s$ (case ND_1) it converges to $(u, v) = (u^s, v^s)$ (cf. Fig. 5b, c). In the former case the solution is clearly not constant, but in the latter case it is easy to show that $(u(\varepsilon^2), v(\varepsilon^2)) \equiv (u^s, v^s)$ for sufficiently small ε . Note that the only property of the glycolytic model that is essential here is that $f = 0$ intersects the u -axis once (it cannot intersect more than once). Thus the conclusions hold for a more general class of mechanisms.

A similar kind of analysis can be done in the cases D_0N and D_1N . However, in these cases there are two branches of solutions that exist at $L = 0$, because the vertical lines $u = \text{constant}$ intersect $g(u, v, p) = 0$ at two points. These intersections are at $(u, v) = (0, 0)$ and $(0, \infty)$ in the case D_0N . We leave it to the reader to derive the leading order terms in these cases.

Next we shall determine the stability of the solutions that exist at small L . First consider the cases ND_1 and D_1N , for which there is the constant solution (u^s, v^s) . In both cases the variational problem relative to this solution consists of the first equation of (5), and the appropriate boundary conditions. The spectral problem is

$$v \mathcal{D} \frac{\partial^2 \Psi}{\partial \zeta^2} + (K - \lambda I) \Psi = 0 \tag{31}$$

$$\begin{aligned} \frac{\partial \Psi_1}{\partial \zeta} &= 0 \\ \Psi_2 &= 0 \end{aligned} \quad \text{at } \zeta = 0, 1 \tag{32}$$

for ND_1 , and (31) plus the boundary conditions

$$\begin{aligned} \Psi_1 &= 0 \\ \frac{\partial \Psi_2}{\partial \zeta} &= 0 \end{aligned} \quad \text{at } \zeta = 0, 1 \tag{33}$$

for D_1N . We assume that $\delta > 0$ and define $\varepsilon^2 \equiv v^{-1}$ as before. Then (31) becomes

$$\begin{bmatrix} 1 & 0 \\ 0 & \delta \end{bmatrix} \frac{\partial^2 \Psi}{\partial \zeta^2} + (\varepsilon^2 K - \bar{\lambda} I) \Psi = 0 \tag{34}$$

where $\bar{\lambda} \equiv \varepsilon^2 \lambda$. At $\varepsilon = 0$ ($L = 0$) the kinetic contribution vanishes, and it is easy to see that the eigenvalues and eigenfunctions for ND_1 are

- (I) $\bar{\lambda} = -(n\pi)^2 \quad \Psi = \begin{pmatrix} \cos n\pi\zeta \\ 0 \end{pmatrix} \quad n = 0, 1, \dots$
- (II) $\bar{\lambda} = -(n\pi)^2 \quad \Psi = \begin{pmatrix} \cos n\pi\zeta \\ \sin n\pi\zeta \end{pmatrix} \quad n = 1, 2, \dots^3$
- (III) $\bar{\lambda} = -\delta(n\pi)^2 \quad \Psi = \begin{pmatrix} 0 \\ \sin n\pi\zeta \end{pmatrix} \quad n = 1, 2, \dots$

The zero eigenvalue is simple and the corresponding eigenfunction is $(1, 0)^T$. In the D_1N case the two components are reversed in the preceding eigenfunctions.

Since $\bar{\lambda} = \varepsilon^2 \lambda$, all but the zero eigenvalue have a pole of order two at $\varepsilon = 0$ ($L = 0$), and therefore the perturbed eigenfunctions corresponding to these eigenvalues lead to decaying solutions for ε sufficiently small. Thus we only have to determine how the zero eigenvalue perturbs for small L . Since the problem is invariant under the transformation $L \rightarrow -L$, the zero eigenvalue cannot pass through zero transversally, and there is no change in stability at $L = 0$.

Because the zero eigenvalue is simple it perturbs smoothly, and we may write

$$\begin{aligned} \bar{\lambda} &= \varepsilon^2 \lambda_1 + \varepsilon^4 \lambda_2 + \dots \\ \Psi &= \Psi_0 + \varepsilon^2 \Psi_1 + \dots, \end{aligned}$$

where $\Psi_0 = (1, 0)^T$ (respectively, $\Psi_0 = (0, 1)^T$) for the case ND_1 (respectively, D_1N). One easily finds that $\lambda_1 = k_{11}$ for ND_1 , and $\lambda_1 = k_{22}$ for D_1N . Since $k_{11} < 0$ and $k_{22} > 0$, it follows that the solution (u^s, v^s) is stable for small L in case ND_1 and unstable for small L in case D_1N .

The three remaining cases are ND_0 , D_0N , and the branch of solutions of D_1N that terminates at (u^s, \bar{v}) , where \bar{v} given by

$$\bar{v} = \frac{1 - \sqrt{1 - 4\kappa(u^s)^2}}{2u^s}.$$

In these cases the basic solution is not constant, and the variational problem has space-dependent coefficients. In particular, the matrix $K = K(\varepsilon^2, \zeta)$ in (34) is

$$K = K_0 + \varepsilon^2 K_1 + \dots = \begin{bmatrix} -\kappa - v^2 & -2uv \\ \kappa + v^2 & 2uv - 1 \end{bmatrix},$$

³ These solutions exist only for $\delta = 1$

Table 2. The stability characteristics of solutions that exist at small L

Case	Basic Solution	Stability Characteristics
ND_0	$(\beta/\kappa, 0)$	Stable
ND_1	(u^s, v^s)	Stable
D_0N	$(0, 0)$	Stable
D_1N	(u^s, v^s)	Unstable
$D_1\bar{N}$	(u^s, \bar{v})	Stable

wherein u and v have the expansions given in (28). In all cases the expansion at order $\mathcal{O}(\varepsilon^2)$ leads to the equation

$$\begin{bmatrix} 1 & 0 \\ 0 & \delta \end{bmatrix} \frac{\partial^2 \Psi_1}{\partial \zeta^2} + (K_0 - \lambda_1 I) \Psi_0 = 0 \tag{35}$$

and therefore λ_1 is given by

$$\lambda_1 = \frac{\langle \Psi_0, K_0 \Psi_0 \rangle}{\langle \Psi_0, \Psi_0 \rangle}. \tag{36}$$

In the case ND_0 , $\Psi_0 = (1, 0)^T$ and $(u_0, v_0) = (\beta/\kappa, 0)$, and one finds that $\lambda_1 = -\kappa$. Since $\kappa > 0$, ND_0 is stable at small L . For D_0N , $\Psi_0 = (0, 1)^T$, $(u_0, v_0) = (0, 0)$, and $\lambda_1 = -1$. Thus D_0N is also stable near $L = 0$. Finally, on the nonuniform branch which terminates at $(u, v) = (u^s, \bar{v})$ in the case D_1N , $\Psi_0 = (0, 1)^T$ and $(u_0, v_0) = (u^s, \bar{v})$. It follows that $\lambda_1 = 2u^s\bar{v} - 1$, which, from the expression above for \bar{v} , is negative. Thus the solutions on this branch are stable for small L .

The conclusions concerning existence and stability of solutions at small L are summarized in Table 2. The interested reader can gain further insight into these results by a direct qualitative analysis of the evolution equations in this limit.

One sees from this table that there are both similarities and differences between scalar and mixed boundary conditions. It follows from the results in [24] and [8] that under homogeneous scalar Neumann conditions the solution $(u, v) = (u^s, v^s)$ of (26) is unique and stable for sufficiently small L , and this is also true for the mixed case ND_1 . However, the same solution is unstable (and not unique) in the mixed case D_1N . One can also show that this solution is stable in the scalar case D_1D_1 , (this follows from the results in [8]), and thus there are several eigenvalue crossings (and possibly bifurcations) as one homotops the boundary conditions around the edges of the face $\Theta_3 = 1$ in Fig. 2. Other differences will emerge from the numerical results described in the following section.

3.3 Linear analysis for general L

As we pointed out in Sect. 2, when the boundary conditions are not scalar conditions, the linear analysis is much more difficult because the eigenfunctions do not have the simple product form. In Appendix A we consider the linear evolution equations associated with (21) for the case D_1N . We show that in this case each eigenfunction is an infinite sum of trigonometric functions and that the growth rate

of each eigenfunction (given by the dispersion relation) is the solution of a generalized eigenvalue problem involving infinite-dimensional matrices. To solve this we consider finite dimensional approximations (FDA) to this infinite dimensional system. We present some examples in A.1 to illustrate the procedure. The convergence properties of the FDA are studied numerically and it appears that for simple types of spatial patterns a low order FDA gives accurate approximations to the full solution. We also show that the spatial eigenfunctions thus calculated agree very closely with the corresponding solution to the steady state problem of the full nonlinear problem as calculated by AUTO (see Sect. 4 and Appendix B).

In A.2 we relate the eigenfunctions of the mixed boundary problem to those of the NN case and in A.3 we illustrate how the FDA procedure can be adapted to locate bifurcation points.

4 Numerical results

In the preceding section we establish the existence of various branches of solutions of the steady-state Eqs. (21) at small L , and determined their stability. In this section we present a more complete picture of the solution set as a function of L , obtained by using numerical continuation and bifurcation techniques. We first present the solutions at six of the eight nodes in the homotopy cube shown in Fig. 2, and compare the properties of the solutions as L varies under the different types of boundary conditions. We then discuss some results obtained by solving the corresponding evolution equations.

The numerical results on steady-state solutions were obtained by discretizing the differential equations using finite differences, and then solving the resulting nonlinear algebraic system using the software package AUTO [11]. The details of the numerical methods used are given in Appendix B.

4.1 Steady state solutions

Figure 6 shows a schematic summary of the primary bifurcation structure as a function of L for various combinations of boundary conditions. For simplicity not all of the solutions are shown in the case D_1N . Some of the similarities and differences that emerge from this figure are as follows.

- The structure of the solution set is quite similar in the cases NN and D_1D_1 , which are the standard Turing cases. In both cases there is a basic constant solution $(u, v) = (u^s, v^s)$, and the bifurcation points on these branches are identical. As we shall see later, the solutions on the primary bifurcating branches are dominated by the mode that changes stability at the corresponding primary bifurcation point. This fact accounts for the principle difference in the spatial distribution of the two components in these cases, for in the NN case the eigenfunctions of the variational problem relative to the basic solution are cosines, whereas in the D_1D_1 case they are sines.
- In four of the six cases shown in this figure, the constant solution $(u, v) = (u^s, v^s)$ exists for all L , and the structure of the solution set is significantly more complex than in the remaining cases. In particular, in the latter cases there are large intervals in which there are no bifurcation points, but as we will see later, the nodal structure

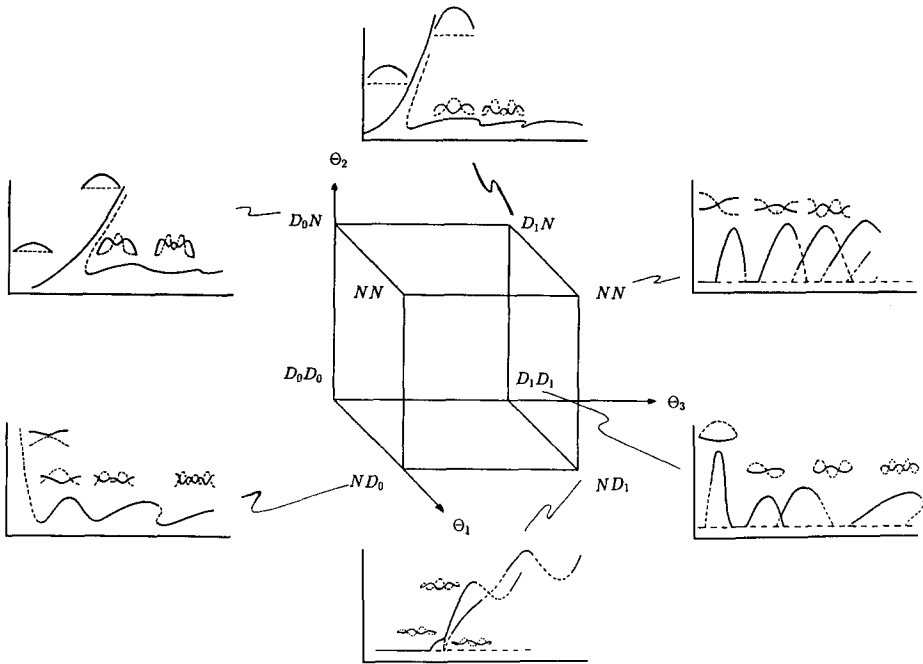


Fig. 6. Schematic illustration of homotopy relationships and a summary of the primary bifurcation structure for different sets of boundary conditions. The detailed bifurcation diagrams and solution profiles for the different cases are presented in the following figures: *NN* (Figs. 7a and 8); *D₁D₁* (Figs. 7b and 9); *ND₁* (Figs. 10 and 11); *D₁N* (Figs. 12 and 13); *D₀N* (Figs. 14 and 15); *ND₀* (Figs. 16 and 17). Here and hereafter we use the following notation. For bifurcation diagrams the horizontal axis is length, *L* (cm), and the vertical axis is the Euclidean norm, $\|(u, v)\|_E$, of the solution vector, where $(u, v) \in R^{82}$. — denotes a stable branch, ---- denotes an unstable branch. For concentration profiles — denotes *u* and ---- denotes *v*

of the solutions can change nonetheless. Thus the imposition of zero boundary conditions on either of the species greatly reduces the admissible types of spatial profiles for the two components. In particular, it will become clear from a later diagram that the solution structure in case *D₀N* is essentially that of case *D₁N*, minus the solutions associated with bifurcations from the basic branch.

The detailed bifurcation diagrams and the spatial profiles of selected solutions associated with the summary given in Fig. 6 are given in Figs. 7–17. These are discussed in the following subsection, but some readers may wish to skip the details and go directly to the summary Sect. 4.3.

4.2 A comparison of the results

As we indicated earlier, the bifurcation points in the *NN* and *D₁D₁* cases can be computed analytically and Table 1 shows a comparison between the analytical and numerical values in these cases. It is clear from the table that the bifurcation points can be located accurately numerically. One can show analytically that the bifurcations are either subcritical or supercritical, i.e., they are all pitchfork bifurcations. In both the *NN* and *DD* cases the nonconstant component of solutions on the *j*th primary bifurcation branch (the branch that bifurcates from the constant solution

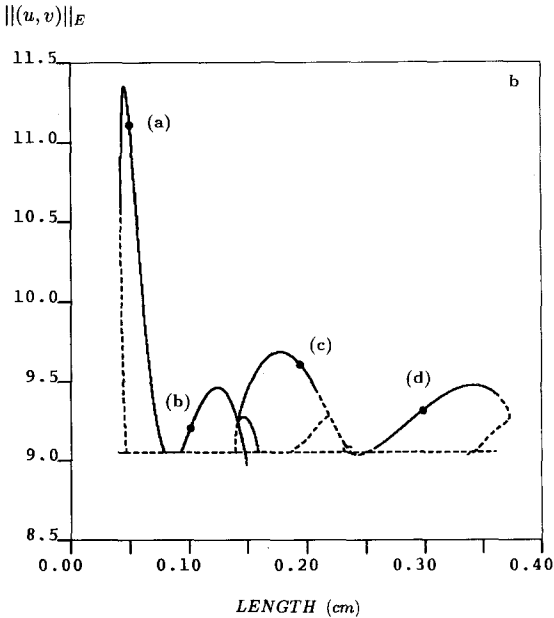
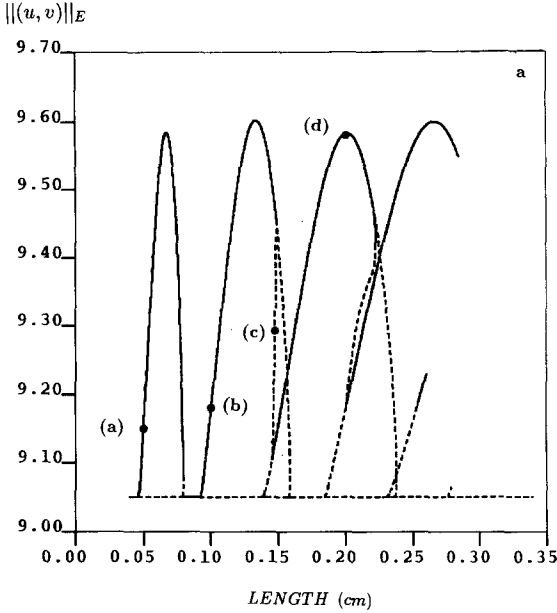


Fig. 7. Bifurcation diagrams for NN (a) and for $D_1 D_1$ (b). Solution profiles at selected points on the bifurcation diagrams are shown in Fig. 8 for NN and in Fig. 9 for $D_1 D_1$. The bifurcation diagram for NN is complete for the first three modes. The horizontal line is the uniform steady state and all other solutions shown bifurcate from it. There is no secondary bifurcation from the first mode; the change in stability on this branch is a turning point. There is a secondary branch connecting modes 2 and 3, and one connecting modes 3 and 4. Note that there is an interval in which stable solutions on the second and third branch coexist, and similarly for the third and fourth branch. There is also a small interval near $L = 0.22$ in which three stable solutions coexist. In the case of $D_1 D_1$ there is a large interval around $L = 0.15$ in which three stable solutions coexist

at L_j^\pm) is dominated by the j^{th} mode. This follows from an asymptotic analysis near the bifurcation points, but holds far from these points as well. To illustrate this, Table 3 shows the amplitudes of the Fourier cosine components for the solutions whose spatial profiles are given in Fig. 8.

In view of this dominance of the unstable mode, it is easy to characterize the nodal structure for each component at a given L , as long as the instability intervals do not overlap. However, one sees in Fig. 7 that the intervals overlap at larger L , as predicted earlier, and that there may be secondary branches of solutions that

Table 3. Dominant Fourier modes of NN for solutions shown in Fig. 8. These are the leading order coefficients ($> 10^{-4}$) for the Fourier cosine series for u and v .

Mode	Length (label)							
	0.05 (a)		0.10 (b)		0.1482 (c)		0.2 (d)	
	u	v	u	v	u	v	u	v
0	1.976E + 00	2.000E + 00	1.976E + 00	2.000E + 00	2.027E + 00	2.000E + 00	2.038E + 00	2.000E + 00
1	-1.311E - 01	3.333E - 01	1.682E - 06	1.452E - 06	-1.360E - 02	5.752E - 03	1.600E - 06	1.738E - 06
2	-1.516E - 03	7.442E - 03	-1.319E - 01	3.349E - 01	-2.389E - 01	3.426E - 01	-1.227E - 06	-2.314E - 06
3			1.200E - 06	2.592E - 06	6.298E - 02	-1.622E - 01	-3.207E - 01	5.411E - 01
4			-1.540E - 03	7.546E - 03	1.847E - 02	6.591E - 02	-2.797E - 06	3.714E - 07
5					-5.408E - 04	2.357E - 03	2.411E - 06	4.635E - 07
6					6.075E - 04	-3.002E - 03	1.033E - 02	-4.057E - 02
7					-1.007E - 03	5.405E - 03	2.255E - 06	1.256E - 07
8							-2.220E - 06	-2.732E - 07
9							2.584E - 03	-1.343E - 02

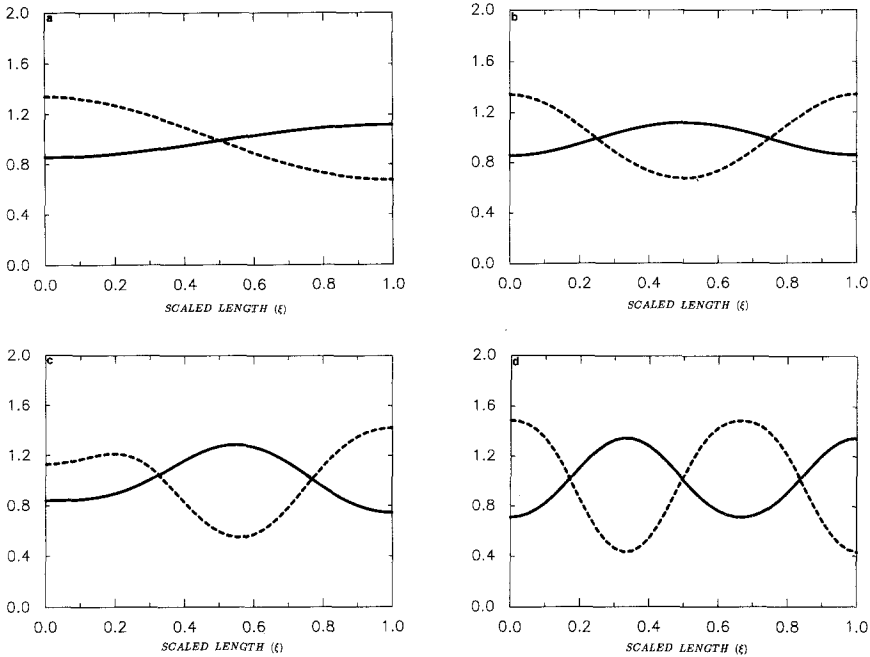


Fig. 8. Panels a–d show the spatial profiles of the solutions at the points labeled a–d in Fig. 7(a). The corresponding L values are 0.05, 0.1, 0.1482, and 0.2, respectively. Solutions on primary bifurcation branches corresponding to even modes are approximately symmetric about $\xi = 0.5$, and solutions on branches corresponding to odd modes are approximately anti-symmetric about $\xi = 0.5$. The solution in panel c, which is a mixed-mode solution on a secondary branch, cannot be characterized as having a uniform phase difference of 0 or π

connect primary branches. On such branches the solution is typically a mix of the dominant modes that characterize the primary branches. An example is given by the solution labelled (c) in Fig. 7, which lies on an unstable secondary branch connecting the second and third primary branches. On the primary branches the spatial gradients are opposed, i.e., $\text{sgn}(u_\xi) = -\text{sgn}(v_\xi)$, but this is not true on secondary branches. Similar statements apply to the other standard Turing case, namely D_1D_1 , and we do not elaborate on this further.

Each of the branches for j odd in Fig. 7 corresponds to two solutions, one of which is transformed into the other under reflection across $\zeta = 1/2$. Of course both of these have the same norm. The two solutions corresponding to j even can be obtained by concatenating solutions for $j/2$ in two combinations. In the continuous problem the L_2 norms of these solutions coincide, but that is not true for the discrete norm used here, because the number of mesh points is fixed. As a result, there is another branch of solutions for j even that is not shown in Fig. 7. In any case, the isotropy group of the solutions on these branches (i.e., the group of symmetry transformations that leaves the solutions invariant), is constant on any connected component of a branch that contains no bifurcation points [25].

The number of primary bifurcation points is significantly reduced if instead of a homogeneous Neumann condition on v one sets $v = v^s$ on the boundary. This is the case ND_1 , for which the bifurcation diagram is shown in Fig. 10. In this case there are only four bifurcation points on the basic solution for $L \in [0, 0.5]$,

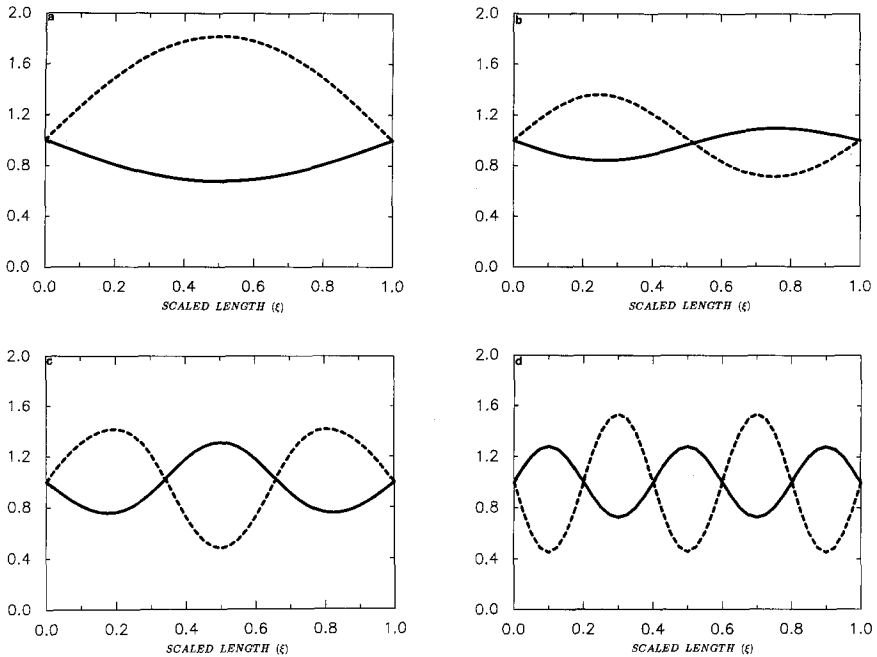


Fig. 9. Panel a–d show the spatial profiles of the solutions at the points labeled a–d in Fig. 7b. The corresponding L values are 0.05, 0.1, 0.2, and 0.3, respectively. On primary branches, even mode solutions are approximately symmetric about $\xi = 0.5$, odd mode solutions are approximately anti-symmetric about $\xi = 0.5$

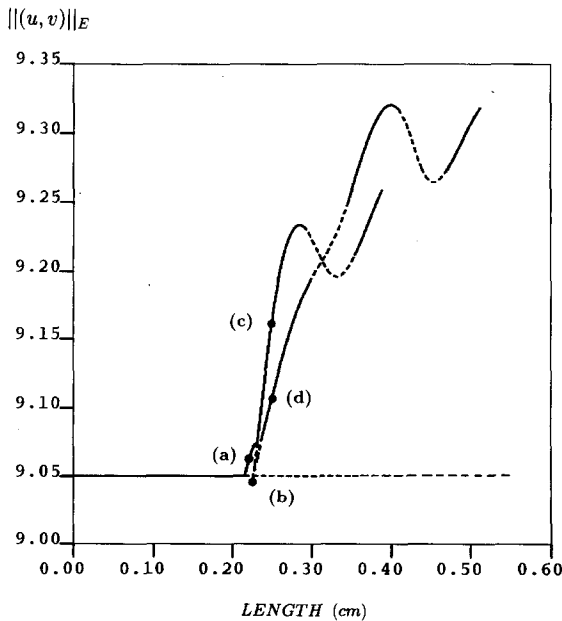


Fig. 10. The bifurcation diagram for ND_1 . There are 2 bifurcation points from the uniform steady state for $L \in (0.04, 0.36)$, one at $L = 0.216$ and the other at $L = 0.226$. The bifurcation branch at $L = 0.216$ is a closed loop that intersects the uniform steady state at only one point. In this profile the branch folds back on itself and returns to the bifurcation point. Solutions for this case at the labeled points are shown in Fig. 11

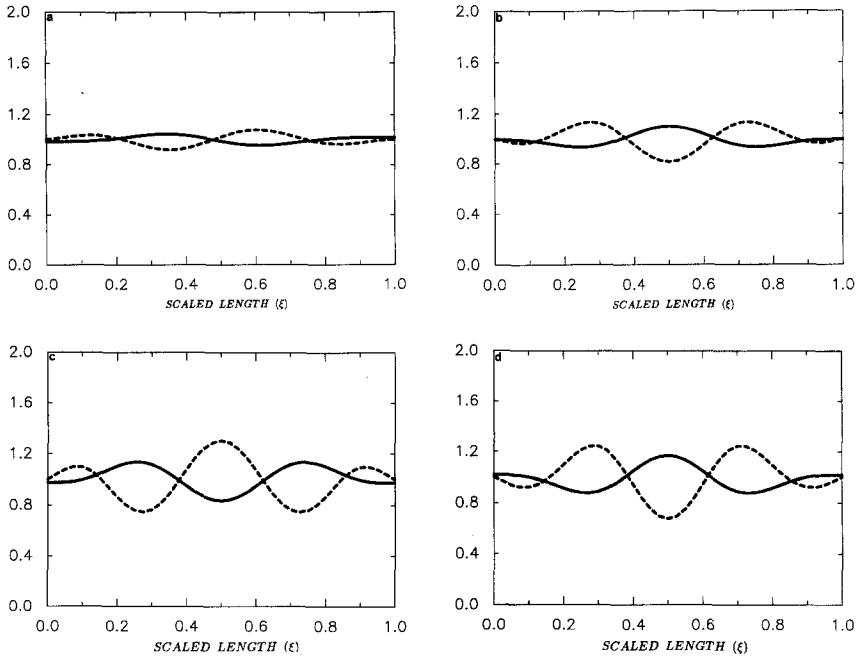


Fig. 11. Panels **a–d** show the spatial profiles of the solutions for ND_1 at the points labeled **a–d** in Fig. 10. In panel **a** $L = 0.219$, in **b** $L = 0.228$, and in **c** and **d** $L = 0.25$

compared with sixteen in either case NN or case D_1D_1 . Furthermore, the global structure of the solution set is much simpler in this range of L than it is in either of the standard Turing cases. Thus two effects of these mixed conditions are that the uniform steady state is stable over a larger L interval, and the solution set is simplified.

Solutions on the first nonuniform branch are approximately, but not precisely, anti-symmetric about $\zeta = 0.5$, whereas on the second branch, solutions are approximately symmetric. If the two equations at (21) were not coupled via the kinetic vectorfield, the eigenfunctions of the variational problem relative to (u^s, v^s) would be of the form $(\cos(n\pi\zeta), \sin(m\pi\zeta))$, and thus it is natural to characterize the nonconstant solutions shown in Fig. 11 in terms of this basis. The results of this representation are shown in Table 4. Solutions (b) and (d), which lie on the same branch, have a similar amplitude spectrum, but those of (a) and (c), which lie on different branches, are quite different. Of course one expects that all these solutions can be characterized in terms of a dominant mode, and in essence the results in the table show which trigonometric functions appear in those modes. As we remarked earlier, one has to solve the coupled system directly to obtain these modes. Several examples of the procedure are given in Appendix A for the case D_1N .

Since the case ND_1 can be obtained from the case NN by a homotopy of one boundary condition, one may ask about the correspondence between bifurcation points and nontrivial solutions in these cases. A generic perturbation of the boundary conditions for a Neumann problem would remove some or all of the

Table 4. Dominant Fourier modes for ND_1 for solutions shown in Fig. 11. These are the leading order coefficients ($> 10^{-4}$) for the Fourier cosine series for u and the Fourier sine series for $v - v^s$

Mode	0.219 (a)			0.228 (b)			0.25 (c)			0.2484 (d)		
	u	$v - v^s$		u	$v - v^s$		u	$v - v^s$		u	$v - v^s$	
0	2.000E + 00	0.000E + 00		1.981E + 00	0.000E + 00		1.977E + 00	0.000E + 00		2.028E + 00	0.000E + 00	
1	4.093E - 03	2.002E - 04		1.615E - 06	-1.614E - 03		1.606E - 06	5.220E - 03		1.625E - 06	-6.652E - 03	
2	4.337E - 03	-2.178E - 02		-3.987E - 02	-8.818E - 08		4.020E - 02	-8.374E - 08		4.077E - 02	9.120E - 08	
3	-3.373E - 02	-9.744E - 03		1.370E - 06	8.432E - 02		1.263E - 06	1.198E - 01		1.980E - 06	-1.283E - 01	
4	-6.284E - 03	5.600E - 02		5.785E - 02	5.923E - 07		1.133E - 01	1.026E - 06		-1.164E - 01	-1.057E - 06	
5	1.227E - 02	1.158E - 02		1.830E - 06	-1.008E - 01		2.159E - 06	-2.027E - 01		1.090E - 06	1.934E - 01	
6	1.413E - 03	-1.058E - 02		-1.251E - 02	-3.611E - 07		-3.546E - 02	-8.893E - 07		2.601E - 02	6.791E - 07	
7	6.498E - 04	-3.611E - 04		1.601E - 06	1.656E - 03		1.594E - 06	2.321E - 02		1.552E - 06	8.477E - 03	
8	1.452E - 04	-2.544E - 03		-1.475E - 03	-9.696E - 08		-2.116E - 03	-1.324E - 07		6.133E - 03	3.122E - 07	
9	1.713E - 04	-5.100E - 05					1.643E - 06	3.334E - 03		1.582E - 06	-3.291E - 03	
10	3.398E - 05	-1.125E - 03					-4.675E - 04	6.956E - 08		1.773E - 03	1.597E - 07	
11							1.659E - 06	-1.491E - 03		1.583E - 06	-2.281E - 03	
12							-7.877E - 04	-1.012E - 07		7.481E - 04	1.069E - 07	
13							1.656E - 06	1.580E - 03		1.589E - 06	-2.095E - 03	

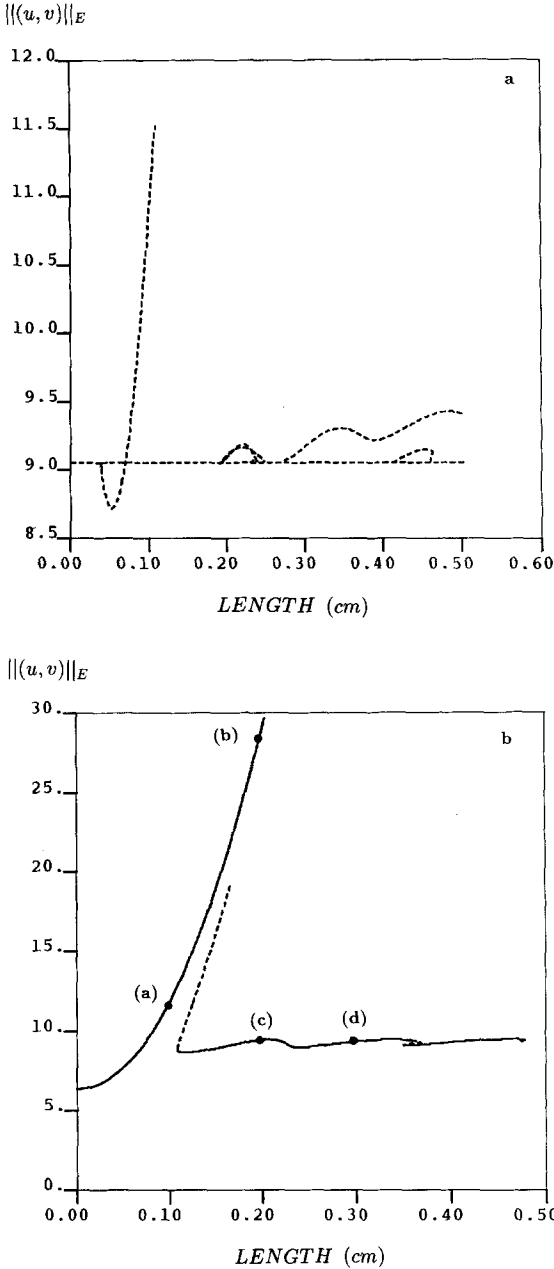


Fig. 12. Bifurcation diagrams for case D_1N . Panel **a** shows solutions that bifurcate from the spatially-uniform steady state, panel **b** shows the continuation of the branch discussed in Sect. 3.

bifurcation points, but here they persist locally in a two-parameter family under a small decrease in the homotopy parameter θ_2 , because the basic solution (u^s, v^s) persists under this homotopy. In Fig. 18 we show the loci traced out in the (L, θ_2) plane by fixed small amplitude solutions that lie near each of the bifurcation points

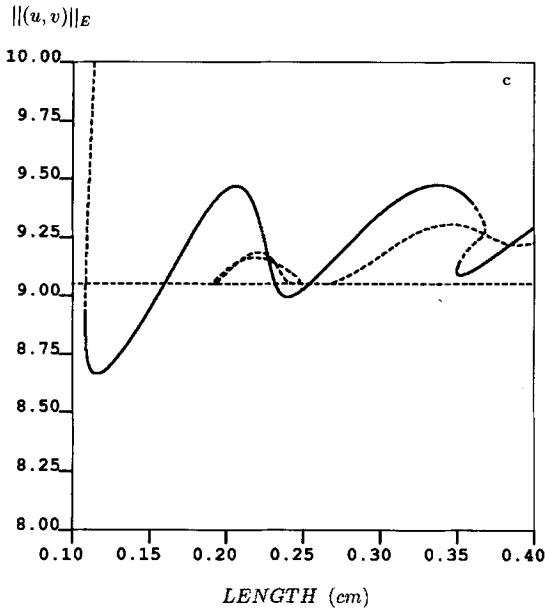


Fig. 12. Bifurcation diagrams for case D_1N . Panel c shows a blow-up of the composite. Solutions at the labeled points are shown in Fig. 13

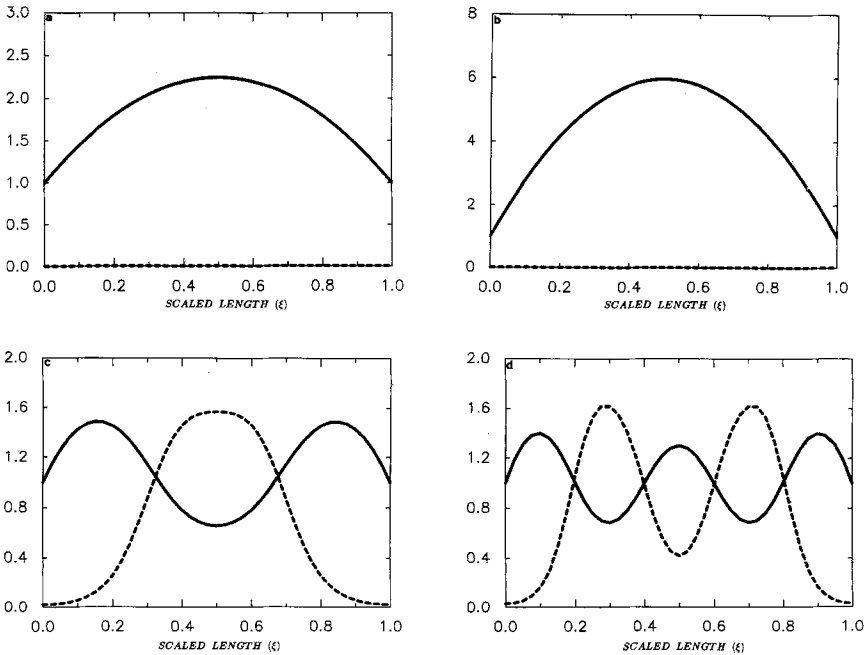


Fig. 13. Panels a–d show the spatial profiles of the solutions for D_1N at the points labeled a–d in Fig. 12b (at $L = 0.1, 0.2, 0.2$, and 0.3 , respectively)

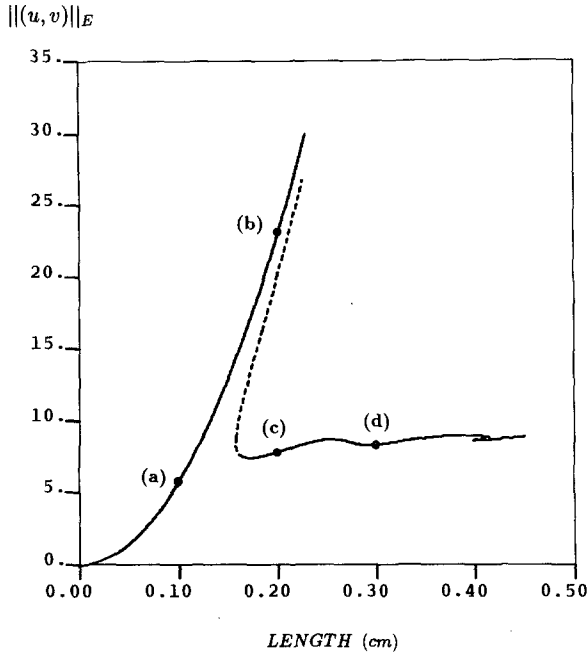


Fig. 14. Bifurcation diagram for the D_0N case. Note the similarity between this diagram and Fig. 12(b)

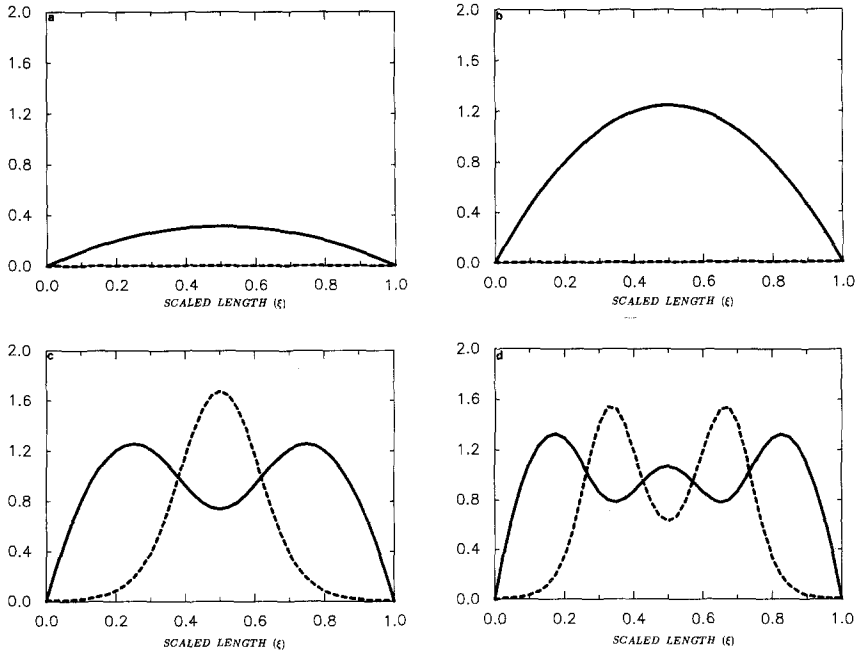


Fig. 15. Panels **a-d** show the spatial profiles of the solutions for D_0N at the points labeled **a-d** in Fig. 14 (at $L = 0.1, 0.2, 0.2,$ and $0.3,$ respectively)

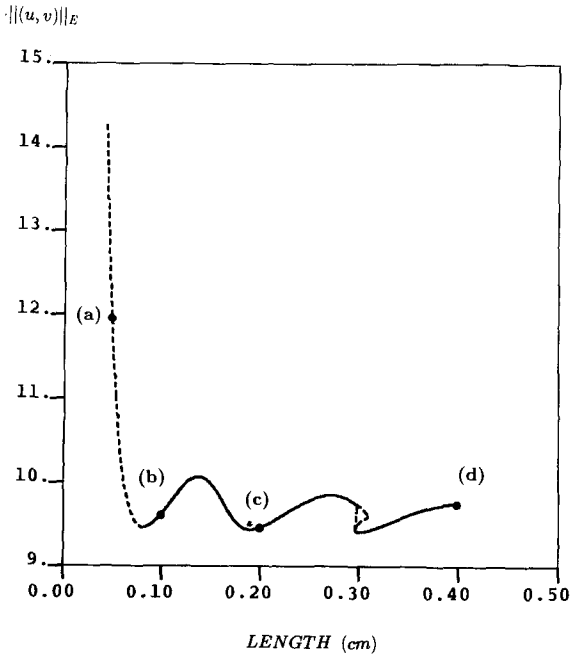


Fig. 16. Bifurcation diagram for the ND_0 case. The global continuation of the branch discussed in Sect. 3 is shown. There are at least two Hopf bifurcation points on this branch, one at $L = 0.00614$, and the other at $L = 0.0812$. Solutions at the labeled points are shown in Fig. 17

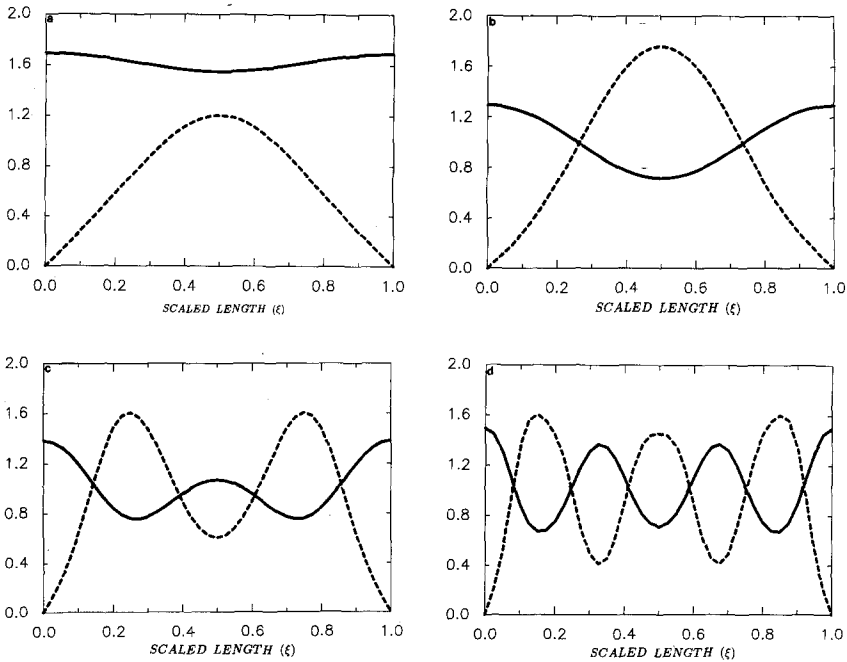


Fig. 17. Panels a-d show the spatial profiles of the solutions for ND_0 at the points labeled a-d in Fig. 16 (at $L = 0.05, 0.1, 0.2$, and 0.4 , respectively)

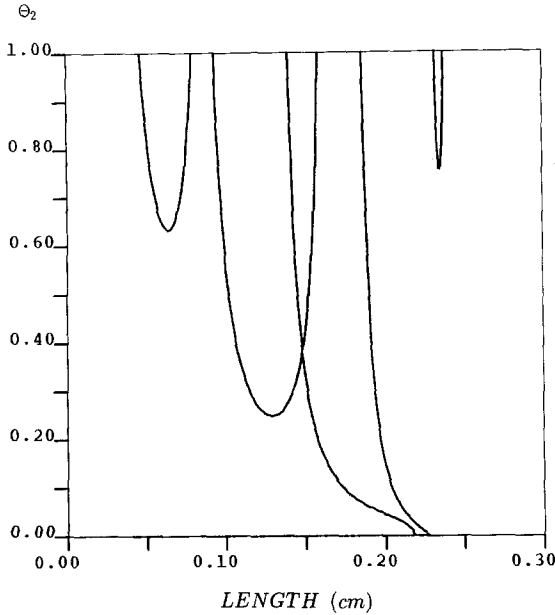


Fig. 18. The locus of bifurcation points on the uniform steady state in the two-parameter $L - \theta_2$ plane. Note that several pairs of bifurcation points that exist in the NN case coalesce as θ_2 is decreased, which leads to a much simpler bifurcation diagram for ND_1 (cf. Figs. 7a and 10)

at $\theta_2 = 1$. To obtain these loci, we augment the algebraic equations obtained by discretizing the partial differential equations with the functional

$$\rho_3 \equiv \int_0^1 \{ [u(\zeta) - u^s]^2 + [v(\zeta) - v^s]^2 \} d\zeta.$$

We then pick a solution near the bifurcation point (with $\rho_3 \sim \mathcal{O}(10^{-10})$), and continue this solution in the two parameters (L, θ_2). We follow this procedure, rather than augment the equations to find zeroes of the determinant of the algebraic system, because following the zeroes of the determinant is numerically very sensitive. Given the above choice of ρ_3 , the results should be indistinguishable in the two approaches, and this was verified by a separate computation at $\theta_2 = 1$. One sees from Fig. 18 that only two bifurcation points continue from case NN to case ND_1 ; the remainder disappear pairwise at intermediate values of θ_2 . Furthermore, in the range of L shown there are no other bifurcation points at $\theta_2 = 0$. In case NN these points correspond to modes three and four, and while these modes are present in the solutions for ND_1 , other modes are present as well. Thus there is little connection between the solutions in these cases.

By contrast with the case ND_1 , in which the mixed condition simplifies the solution set as a function of L , imposing the Dirichlet condition on u has the opposite effect. One sees in Fig. 12 that there are two disjoint components of the solution set, one comprising solutions connected with the uniform steady state, and another comprising solutions that are connected with the stable non-constant solution that was discussed in Sect. 3. The second set is more interesting than the first, because there are stable solutions for all $L > 0$ on it. One may again investigate the correspondence between these solutions and those in case NN , and the results are shown in Fig. 19. The procedure for the continuation is the same as

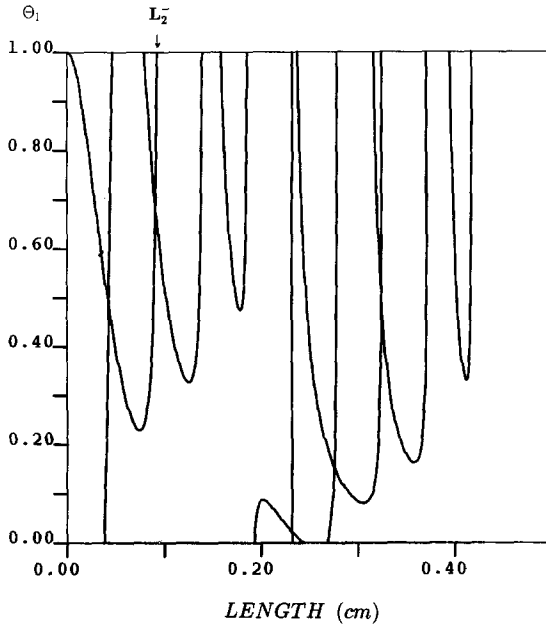


Fig. 19. A homotopy of the bifurcation points between case NN $((\theta_1, \theta_2, \theta_3) = (1, 1, 1))$ and D_1N $((\theta_1, \theta_2, \theta_3) = (0, 1, 1))$. The curves show the locus of bifurcation points on the uniform steady state as θ_1 varies. There is a codimension-two bifurcation point at $(0, 1)$, and one curve of bifurcation points emanating from there terminates at L_2 .

used previously, and it succeeds for the same reason as before. One sees that in the range $L \in (0, 0.4)$ only three of the fourteen bifurcation points that exist in case NN continue to case D_1N . In addition, there are two bifurcation points on the basic solution for D_1N that are not connected to bifurcation points for NN .

Spatial profiles of the solutions labelled (a)–(d) in Fig. 12 are shown in Fig. 13, and the amplitude spectrum of these solutions relative to the basis $\{(\sin(m\pi\zeta), \cos(n\pi\zeta))\}$ is given in Table 5. The solutions labelled (a) and (b) have $v \approx 0$, and $u \approx k \sin \pi\zeta$ for some constant k . Solutions such as (c) and (d) are characterized by a few cosine modes in u and a few sine modes in v . Generally speaking, u is dominated by a few even cosine modes whereas v is dominated by a few odd sine modes in case D_1N .

The transition from D_1N to D_0N involves a homotopy in θ_3 . One sees from a comparison of Figs. 12 and 14 that this transition prunes off all solutions connected with the basic solution (u^s, v^s) . The profiles along the remaining branch are remarkably similar at the same L values, except that in case D_0N u is pinned at zero at the endpoints, rather than at u^s (cf. Figs. 13 and 15).

The last case considered is ND_0 , which can be gotten from case NN via a homotopy in θ_2 . One sees from the bifurcation diagram for this case (cf. Fig. 16) that there is no apparent connection between the structure of the solution set in this case and that in any of the other cases. The main branch shown in Fig. 16 begins at the point $(u, v) = (\beta/\kappa)$, at $L = 0$, as was shown in Sect. 3 (cf. Fig. 5b). There are Hopf bifurcation points on this branch at $L = 0.00614$ and $L = 0.0812$, and periodic solutions bifurcate at these points. The periodic solutions are nearly synchronized in space and are qualitatively similar to the periodic solutions that exist in the local dynamics at a slightly larger value of β (cf. [1]). Aside from the short secondary branch which shortcuts the turn in the main branch at about

Table 5. Dominant Fourier modes for D, N for solutions shown in Fig. 12(b) on the component not containing the uniform solution (u^s, v^s). These are the leading order coefficients ($> 10^{-2}$) from the Fourier sine series for $u - u^s$ and the Fourier cosine series for v

Mode	0.1 (a)		0.2 (b)		0.2 (c)		0.3 (d)	
	$u - u^s$	v	$u - u^s$	v	$u - u^s$	v	$u - u^s$	v
0	0.000E + 00	3.673E - 03	0.000E + 00	8.844E - 03	0.000E + 00	1.376E + 00	0.000E + 00	1.622E + 00
1	1.287E + 00	3.047E - 09	5.134E + 00	8.183E - 09	5.329E - 02	1.544E - 06	1.241E - 02	1.588E - 06
2			5.109E - 06	-1.868E - 03	-8.527E - 07	-8.385E - 01	-3.466E - 07	-4.114E - 01
3			1.909E - 01	2.457E - 09	4.484E - 01	-1.643E - 06	3.361E - 02	1.308E - 06
4					1.085E - 06	1.413E - 01	-1.227E - 06	-6.397E - 01
5							3.523E - 01	-3.212E - 06
6							1.387E - 06	2.179E - 01

$L = 0.3$, there is in fact a single branch of time-independent solutions in the range of L shown. Solutions on this branch can change their nodal structure without passing through a bifurcation point. We can characterize the “mode” for solutions of ND_0 , by the number of connected components in $[0, 1]$ in which $v > u$. In this way the “mode” numbers increase with L . The solution at $L = 0.05$ is “mode” 0, the solution at $L = 0.1$ is “mode” 1, the solution at $L = 0.2$ is “mode” 2, while that at $L = 0.4$ is “mode” 3. Except for a short interval at about $L = 0.3$, the “modes” do not overlap, i.e., over a large range of L there is only one stable solution. In comparison with the NN case, the problem of multiple stable solutions for a given L is greatly reduced.

4.3 Summary

Several important conclusions can be drawn from these results, and we summarize them as follows.

(i) Nodal structure of solutions: Tables 4–7, for the cases ND_1 , D_1N , D_0N and ND_0 , respectively, show that the spatial distribution of the species which satisfies Neumann conditions is dominated by cosine modes, while the species which satisfies Dirichlet conditions is dominated by sine modes. Imposing Dirichlet conditions on one species appears, in many cases, to reduce the anti-symmetric (odd cosine) mode components of the species which satisfies a Neumann condition (see Tables 4–7). The concentration profiles are not precisely symmetric about $\zeta = 0.5$ due to the higher order modes of the nonlinear problem and to the presence of the anti-symmetric modes. Comparison with linear analysis for some typical cases is made in Appendix A.1, Examples 4 and 5, and the relationship with the NN case is discussed in Appendix A.2. The linear analysis done in Appendix A predicts that eigenfunctions containing odd (even) sine components in the Dirichlet species are coupled with those in the Neumann species that contain even (odd) cosine components.

(ii) Symmetry properties: In Sect. 2 (Proposition 5) we proved that for a kinetic mechanism of global cross activator-inhibitor type with Neumann boundary conditions on both species the nonconstant solution profiles are out of phase, at least in the vicinity of a primary bifurcation point. Our numerical solutions confirm this, but Fig. 8c shows that this does not necessarily hold on secondary bifurcation branches.

(iii) In the case of mixed boundary conditions it becomes meaningless to talk of phase differences, since one is then comparing the several dominant cosine modes of the Neumann species with the several dominant sine modes of the Dirichlet species (see for example, Figs. 13, 15, and 17). However, in this case, a maximum of one species almost coincides with a minimum of the other species. This is also true for the NN case and appears to be a general property of a kinetic mechanism of global cross activator-inhibitor type that holds regardless of the boundary conditions imposed.

(iv) Complexity of the bifurcation diagram: The complexity of the bifurcation behavior of the system can be greatly reduced by changing the boundary conditions. For example, over the interval $L \in (0, 0.5)$ there are sixteen bifurcation points from the uniform steady state for the NN case (Fig. 7) but only four bifurcation

Table 6. Dominant Fourier modes for $D_0 N$ for solutions shown in Fig. 15. These are the leading order coefficients ($> 10^{-2}$) from the Fourier sine series for u and the Fourier cosine series for v

Mode	0.1 (a)		0.2 (b)		0.2 (c)		0.3 (d)	
	u	v	u	v	u	v	u	v
0	0.000E + 00	1.665E - 03	0.000E + 00	6.747E - 03	0.000E + 00	9.984E - 01	0.000E + 00	1.314E + 00
1	1.289E + 00	1.524E - 09	5.139E + 00	6.471E - 09	1.276E + 00	1.174E - 06	1.265E + 00	1.416E - 06
2			5.115E - 06	- 1.831E - 03	3.950E - 07	- 7.435E - 01	8.960E - 08	- 6.306E - 01
3			1.911E - 01	8.704E - 10	5.021E - 01	- 1.994E - 06	5.373E - 01	- 3.509E - 07
4					1.950E - 06	3.310E - 01	9.507E - 07	- 2.847E - 01
5							3.069E - 01	- 2.660E - 06
6							2.413E - 06	3.608E - 01

Table 7. Dominant Fourier modes for ND_0 for solutions shown in Fig. 17. These are the leading order coefficients ($> 10^{-2}$) for the Fourier cosine series for u and the Fourier sine series for v

Mode	0.05 (a)		0.1 (b)		0.2 (c)		0.4 (d)	
	u	v	u	v	u	v	u	v
0	3.246E + 00	0.000E + 00	2.026E + 00	0.000E + 00	0.999E + 00	0.000E + 00	2.065E + 00	0.000E + 00
1	2.582E - 06	1.120E + 00	1.478E - 06	1.538E + 00	1.508E - 06	1.367E + 00	1.634E - 06	1.299E + 00
2			2.919E - 01	2.112E - 06	1.491E - 01	4.769E - 07	2.184E - 02	8.121E - 08
3			2.499E - 06	-2.339E - 01	1.560E - 06	6.219E - 01	1.476E - 06	5.186E - 01
4					2.328E - 01	3.204E - 06	2.049E - 02	2.122E - 07
5					2.911E - 06	-2.154E - 01	3.987E - 07	6.063E - 01
6							3.692E - 01	4.848E - 06
7							3.778E - 06	-1.945E - 01

points for the ND_1 case (Fig. 10). The reduction in the number of primary bifurcation points as θ_2 homotopies from NN to ND_1 is illustrated in Fig. 18, which shows that as θ_2 decreases some pairs of bifurcation points coalesce into a single point, which then disappears. Others drift to the right with L . Hence fixing $v = v^s$ at the boundary increases the range in L over which the uniform steady state is stable. Figure 19 shows that the number of primary bifurcation points also decreases as one homotopies from NN to D_1N . Along with the reduction in the number of bifurcation points, changing the boundary conditions to mixed type can reduce the multiplicity of stable solutions. For example, in the ND_0 case there is only one stable solution over a large range of L . Furthermore, there is only a very short range of L over which multiple solutions exist, and these are not stable. This is graphically illustrated in Fig. 20.

(v) Behavior at small L : In the NN case, a minimum domain length is required for a nonconstant steady state solution to exist (Sect. 2.2 and Fig. 7). However, for the mixed boundary problem D_1N , we showed in Sect. 3 that the constant solution is unstable at arbitrarily small L , and that there is a stable nonconstant solution at small L (cf. Fig. 13). In cases D_0N and ND_0 there is no constant solution, but in each case there is a stable nonconstant solution at sufficiently small L .

5 Discussion

Since the seminal paper of Turing in 1952, a large number of Turing-type models have been proposed for spatial pattern formation. It has been shown that such models exhibit a great variety of spatially patterned solutions and their properties have been widely studied mathematically, while the mechanisms have been extensively proposed to account for spatial pattern formation in a number of developmental contexts. Although these models exhibit a bewildering range and complexity of patterns, nature appears to select only a relatively small number of these patterns. Therefore the essential feature of any realistic model for development is not so much that of pattern generation but that of carefully selecting a small number of patterns in a robust and controlled manner. It is already well-known that in Turing models, the pattern selection process is very sensitive to initial conditions, scale, geometry, and parameter variation. As they stand, therefore, Turing models are inadequate to account for robust patterning mechanisms such as those that underlie, for example, the development of skeletal patterns in the tetrapod limb.

In this paper we have shown that in one space dimension the properties of the solutions of a reaction-diffusion system can be profoundly affected by the nature of the boundary conditions. In particular, we have shown that imposing nonscalar boundary conditions can lead, in a robust and controlled manner, to a sequence of transitions that closely resembles those observed in skeletal patterning in the developing limb, as shown in Fig. 20. We took the domain length L as the bifurcation parameter in this study. However, as this parameter occurs in a dimensionless group that involves diffusion coefficients and a characteristic reaction time, the sequence of transitions shown in Fig. 20 could be generated in other ways. For example, it could arise from a change in the permeability of gap junctions between the cells [5], which in a continuum description is reflected in a change in the diffusion coefficients [29]. This possibility has recently been incorporated in a two-dimensional model of limb development [10].

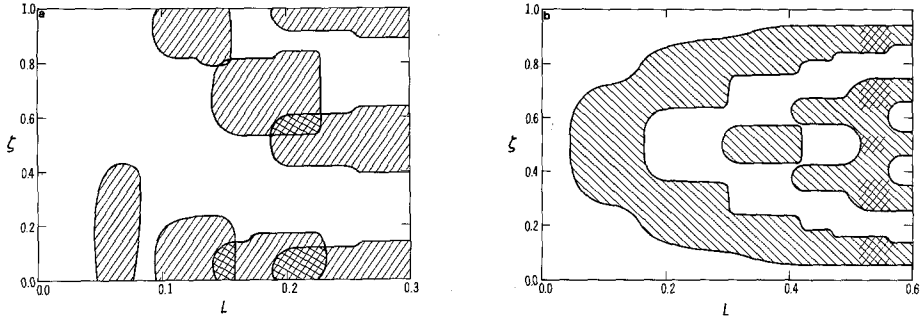


Fig. 20. *a, b* Shown here are the subintervals of $(0, 1)$ in which the v -component of the solution exceeds a fixed threshold, as a function of the length L . *a* Case NN , *b* Case ND_0 . In *a* only one of the pairs of solutions which exist at each L is shown. It is clear from *b* that a simple threshold mechanism can reliably produce the sequence $1, 2, \dots$ of pattern elements as the length increases, whereas this is impossible for the standard Turing model, as shown in *a*

Note that our model solutions capture neither the anterior-posterior spatial asymmetries observed in the skeletal elements of the limb nor their temporal sequence of development along this axis. Recently, Benson et al. [3, 4] have shown that a spatially varying diffusion coefficient can produce such spatial asymmetry. The temporal sequence of pattern formation may be due to cells responding to the spatial pattern in a time-specific fashion.

Computations not reported here show that nonscalar boundary conditions also lead to pattern formation for a much larger ratio of diffusion coefficients than in the scalar case, thereby enlarging the parameter domain over which certain patterns exist and hence lowering pattern sensitivity to small changes in the environment. A further consequence of nonscalar boundary conditions is that, depending on the exact form of the conditions, the model can exhibit stable, spatially nonuniform patterns at very small lengths. This is in contrast to the Turing model, which only exhibits the spatially uniform steady state in this limit.

In summary, boundary conditions have a marked affect on the patterns exhibited by reaction-diffusion models in one space dimension. We would expect this effect to be even more pronounced in two- and three-dimensions, because in these cases one has an even wider choice of different types of boundary conditions.

A Appendix

A.1 Linear stability analysis

In this appendix we consider the variational equation associated with (11) in more detail. We write it in the form

$$\begin{aligned} \frac{\partial \xi_1}{\partial \tau} &= v \frac{\partial^2 \xi_1}{\partial \zeta^2} + k_{11} \xi_1 + k_{12} \xi_2 \\ \frac{\partial \xi_2}{\partial \tau} &= \delta v \frac{\partial^2 \xi_2}{\partial \zeta^2} + k_{21} \xi_1 + k_{22} \xi_2, \end{aligned} \quad \zeta \in (0, 1) \tag{37}$$

and we first consider the boundary conditions

$$\xi_1 = 0, \frac{\partial \xi_2}{\partial \zeta} = 0, \text{ at } \zeta = 0, 1 \tag{38}$$

which correspond to case D_1N . Recall that we know from Sect. 3 that the spatially-uniform steady state (u^s, v^s) is unstable at small L in this case. (Recall that there is also a nonconstant, stable solution in this case.)

Since the boundary conditions are not scalar conditions, the eigenfunctions do not have a simple product form. However, functions that vanish at the endpoints have a sine expansion and those with a vanishing derivative at the endpoints have a cosine expansion. Therefore, (37) and (38) have solutions of the form

$$\begin{pmatrix} \xi_1 \\ \xi_2 \end{pmatrix} = e^{\lambda t} \Phi$$

where

$$\Phi = \begin{pmatrix} \sum_{m=1}^{\infty} A_m \sin(m\pi\zeta) \\ \sum_{n=0}^{\infty} B_n \cos(n\pi\zeta) \end{pmatrix}. \tag{39}$$

By contrast, in the classical linear problem with scalar homogeneous Neumann conditions, the n^{th} eigenfunction is of the form

$$\Phi = \begin{pmatrix} A_n \\ B_n \end{pmatrix} \cos(n\pi\zeta). \tag{40}$$

Substituting (39) into (37) we obtain

$$\begin{aligned} \sum_{m=1}^{\infty} [\lambda + v(m\pi)^2 - k_{11}] A_m \sin(m\pi\zeta) &= \sum_{n=0}^{\infty} k_{12} B_n \cos(n\pi\zeta) \\ \sum_{n=0}^{\infty} [\lambda + v\delta(n\pi)^2 - k_{22}] B_n \cos(n\pi\zeta) &= \sum_{m=1}^{\infty} k_{21} A_m \sin(m\pi\zeta). \end{aligned} \tag{41}$$

Multiplying through by $\sin(m\pi\zeta)$ and integrating over $[0, 1]$ leads to

$$\begin{aligned} [\lambda + v(m\pi)^2 - k_{11}] A_m &= \sum_{n=0}^{\infty} k_{12} B_n \alpha_{nm} \\ k_{21} A_m &= \sum_{n=0}^{\infty} [\lambda + v\delta(n\pi)^2 - k_{22}] B_n \alpha_{nm} \end{aligned} \tag{42}$$

where

$$\alpha_{nm} = \frac{\langle \cos(n\pi\zeta), \sin(m\pi\zeta) \rangle}{\langle \sin(m\pi\zeta), \sin(m\pi\zeta) \rangle} \text{ and } \langle f, g \rangle = \int_0^1 f(\zeta)g(\zeta)d\zeta.$$

System (42) is an infinite system of linear equations for the infinite number of unknowns $A_m, B_n, m = 1, 2, 3, \dots, n = 0, 1, 2, 3, \dots$. To solve this system we make a finite dimensional approximation (FDA) to it by considering only values of m up to M and truncating the sums at $n = M - 1$. This leads to a system of $2M$

equations for the $2M$ unknowns $(A_1, A_2, \dots, A_M, B_0, B_1, \dots, B_{M-1})$. We may rewrite the truncated system as the generalized eigenvalue problem

$$P\mathbf{x} = \lambda Q\mathbf{x} \tag{43}$$

where $\mathbf{x} = (A_1, A_2, \dots, A_M, B_1, \dots, B_{M-1})$ and P and Q are $2M \times 2M$ matrices which have the block structure

$$P \equiv \begin{bmatrix} P_1 & P_2 \\ P_3 & P_4 \end{bmatrix}, \quad Q \equiv \begin{bmatrix} -I & 0 \\ 0 & Q_4 \end{bmatrix}.$$

Here P_i and Q_i are $M \times M$ matrices given by

$$\begin{aligned} (P_1)_{ij} &= \begin{cases} 0 & \text{if } i \neq j \\ v(m\pi)^2 - k_{11} & \text{if } i = j \end{cases} \\ (P_2)_{ij} &= -k_{12}\alpha_{j-1,i} & P_3 &= k_{12}I \\ (P_4)_{ij} &= (v\delta(j-1)^2\pi^2 - k_{22})\alpha_{j-1,i} \\ (Q_4)_{ij} &= \alpha_{j-1,i} \end{aligned}$$

where $i, j = 1, 2, \dots, M$, and I is the $M \times M$ unit matrix.

The solution of (43) leads to $2M$ eigenvalues λ_i with corresponding eigenvectors \mathbf{x}_i . Thus the M -dimensional approximation to the solution of (37) and (38) is

$$\begin{pmatrix} \xi_1 \\ \xi_2 \end{pmatrix} = \sum_{i=1}^{2M} \begin{pmatrix} \sum_{m=1}^M A_{mi} \sin(m\pi\zeta) \\ \sum_{n=0}^{M-1} B_n \cos(n\pi\zeta) \end{pmatrix} e^{\lambda_i \tau} \tag{44}$$

where $(A_{1i}, A_{2i}, \dots, A_{Mi}, B_{0i}, B_{1i}, \dots, B_{(M-1)i})$ is the eigenvector with eigenvalue λ_i .

As the dimension of the FDA is increased, the values of the previously calculated eigenvalues and eigenvectors will change and more eigenvalues and corresponding eigenvectors will be generated. We use the following criteria as stopping tests.

(i) The approximation for a chosen λ_i and its corresponding eigenvector must converge as the dimension of the FDA is increased. In the case of the eigenvectors this also means that higher order terms are insignificant. For any given λ there is an M_c such that the computed eigenvalue and eigenvector are sufficiently accurate for $M = M_c$.

(ii) The eigenvalues introduced for $M > M_c$ have real part negative, and thus correspond to temporally decaying solutions of (37).

If both these criteria are satisfied, then we are assured that the FDA only ignores exponentially decaying terms in time and insignificantly small terms in the trigonometric expansion of the spatial component of the solution to (37). Furthermore, if some of the eigenvalues obtained by the FDA have positive real part, then the uniform steady state of (37) is unstable and we postulate that the solution will evolve to a spatially varying solution of the form (44) with temporal growth rates given by the real part of the positive eigenvalues.

To solve the generalized eigenvalue problem (43) we use the NAG library routine F02BJF which essentially reduces both matrices to triangular form by a coordinate transformation, solves the eigenvalue problem in the new coordinate system, then transforms the eigenvectors thus obtained back to the original coordinate system (see [21, 35]). We can test the accuracy of our analytic approximation in several ways.

1. We can solve the linear partial differential equation system (37) with the boundary conditions (38) using the NAG library routine D03PGF (which is based on a method of lines procedure and uses Gear’s method to integrate the resulting system of ordinary differential equations) to obtain the actual values of ξ_1 and ξ_2 . We can then calculate the Fourier sine and cosine series for ξ_1 and ξ_2 respectively and compare them to the predictions made above. Furthermore, we can calculate the linear growth rate of solutions and compare them with the positive eigenvalues from the FDA. We carried this test out on a large number of examples and, in every case, we found very good agreement between the analytical predictions and the corresponding numerical solutions.

2. Since (37) is the linearization about a uniform steady state of the nonlinear system (4), the FDA scheme gives a linear approximation to the full nonlinear problem. Whenever the linear analysis predicts exponentially growing solutions we cannot compare growth rates of the two solutions, but we can compare the eigenfunctions of the positive (unstable) eigenvalues with Fourier sine and cosine decomposition of the solution to the nonlinear steady state problem as calculated from AUTO.

We illustrate the FDA procedure with two examples for the glycolysis model (25) with $\delta = 0.14$ and the other parameter values fixed as stated:

Example 1. With boundary condition (38) (the D_1N case in Sect. 4) and $L = 0.052$, there are two growing modes and the linear analysis predicts the solution

$$\begin{pmatrix} \xi_1 \\ \xi_2 \end{pmatrix} = C_1 \begin{pmatrix} \sin \pi\zeta + 0.06 \sin 3\pi\zeta \\ -1.09 - 0.02 \cos 2\pi\zeta + 0.01 \cos 4\pi\zeta \end{pmatrix} e^{\lambda_1\tau} \\ + C_2 \begin{pmatrix} \sin 2\pi\zeta + 0.10 \sin 4\pi\zeta + 0.03 \sin 6\pi\zeta \\ -9.5 \cos \pi\zeta - 0.1 \cos 3\pi\zeta - 0.01 \cos 5\pi\zeta \end{pmatrix} e^{\lambda_2\tau}$$

to within terms of $\mathcal{O}(10^{-2})$. Here $\lambda_1 = 0.70$, $\lambda_2 = 0.39$, and $C_1 = 0.42$, $C_2 = 0.11$, all to the same order. On the other hand, the steady state solution to the full nonlinear system is

$$\begin{pmatrix} u \\ v \end{pmatrix} = C_1 \begin{pmatrix} \sin \pi\zeta \\ -1.23 - 0.08 \cos 2\pi\zeta \end{pmatrix} + C_2 \begin{pmatrix} \sin 2\pi\zeta \\ -11.79 \cos \pi\zeta \end{pmatrix}$$

to the same order.

Example 2. Suppose that the boundary conditions are $\partial\xi_1/\partial\zeta = 0 = \xi_2$ at $\zeta = 0, 1$, which correspond to the ND_1 case of Sect. 4. We consider different values of L .

(a) $L = 0.219$. The solution of the linear problem to leading order is

$$\begin{pmatrix} \xi_1 \\ \xi_2 \end{pmatrix} = C_1 \begin{pmatrix} -0.13 \cos \pi\zeta + \cos 3\pi\zeta - 0.36 \cos 5\pi\zeta - 0.16 \cos 7\pi\zeta \\ 0.65 \sin 2\pi\zeta - 1.67 \sin 4\pi\zeta + 0.33 \sin 6\pi\zeta + 0.07 \sin 8\pi\zeta \end{pmatrix} e^{\lambda_1\tau},$$

where $\lambda_1 = 2.17 \times 10^{-4}$ and $C_1 = 0.47$. The corresponding solution to the steady state problem of the full nonlinear system, as calculated using AUTO, is

$$\begin{pmatrix} u \\ v \end{pmatrix} = C_1 \begin{pmatrix} \cos 3\pi\zeta - 0.36 \cos 5\pi\zeta \\ 0.65 \sin 2\pi\zeta - 1.67 \sin 4\pi\zeta + 0.31 \sin 6\pi\zeta \end{pmatrix} + C_2 \begin{pmatrix} 0 \\ \sin 5\pi\zeta \end{pmatrix}$$

to leading order.

(b) $L = 0.228$: Linear analysis yields the solution

$$\begin{pmatrix} \xi_1 \\ \xi_2 \end{pmatrix} = C_1 \begin{pmatrix} 0.11 + \cos 2\pi\zeta - 1.37 \cos 4\pi\zeta + 0.25 \cos 6\pi\zeta + 0.04 \cos 8\pi\zeta \\ 0.05 \sin \pi\zeta - 2.06 \sin 3\pi\zeta + 2.29 \sin 5\pi\zeta + 0.05 \sin 7\pi\zeta \end{pmatrix} e^{\lambda_1 \tau} \\ + C_2 \begin{pmatrix} -0.05 \cos \pi\zeta + \cos 3\pi\zeta - 0.42 \cos 5\pi\zeta - 0.01 \cos 7\pi\zeta \\ 0.57 \sin 2\pi\zeta - 1.67 \sin 4\pi\zeta - 0.43 \sin 6\pi\zeta + 0.08 \sin 8\pi\zeta \end{pmatrix} e^{\lambda_2 \tau}$$

where $\lambda_1 = 4.62 \times 10^{-5}$, $\lambda_2 = 4.95 \times 10^{-3}$, and $C_1 = 0.28$, $C_2 = -0.47$. The steady state solution of the nonlinear system is

$$\begin{pmatrix} u \\ v \end{pmatrix} = C_1 \begin{pmatrix} \cos 2\pi\zeta - 1.45 \cos 4\pi\zeta + 0.31 \cos 6\pi\zeta \\ -2.11 \sin 3\pi\zeta + 2.53 \sin 5\pi\zeta \end{pmatrix}$$

to leading order.

(c) $L = 0.230$: Linear analysis predicts that

$$\begin{pmatrix} \xi_1 \\ \xi_2 \end{pmatrix} = \begin{pmatrix} 0.11 + \cos 2\pi\zeta - 1.33 \cos 4\pi\zeta + 0.28 \cos 6\pi\zeta + 0.04 \cos 8\pi\zeta \\ 0.03 \sin \pi\zeta - 2.1 \sin 3\pi\zeta + 2.0 \sin 5\pi\zeta + 0.04 \sin 7\pi\zeta \end{pmatrix} e^{\lambda_1 \tau} \\ + C_2 \begin{pmatrix} -0.04 \cos \pi\zeta + \cos 3\pi\zeta - 0.43 \cos 5\pi\zeta - 0.01 \cos 7\pi\zeta \\ 0.55 \sin 2\pi\zeta - 1.68 \sin 4\pi\zeta + 0.47 \sin 6\pi\zeta + 0.09 \sin 8\pi\zeta + 0.04 \sin 10\pi\zeta \end{pmatrix} e^{\lambda_2 \tau}$$

where $\lambda_1 = 2.71 \times 10^{-3}$, $\lambda_2 = 6.00 \times 10^{-3}$, and $C_1 = 0.27$, $C_2 = 0.47$. The steady state solution of the nonlinear system is

$$\begin{pmatrix} u \\ v \end{pmatrix} = C_1 \begin{pmatrix} \cos 2\pi\zeta - 1.52 \cos 4\pi\zeta \\ -2.2 \sin 3\pi\zeta + 2.6 \sin 5\pi\zeta \end{pmatrix} + C_2 \begin{pmatrix} \cos 3\pi\zeta - 0.40 \cos 5\pi\zeta \\ 0.55 \sin 2\pi\zeta - 1.6 \sin 4\pi\zeta + 0.34 \sin 6\pi\zeta \end{pmatrix}$$

to leading order.

These two examples show that linear analysis provides a reasonable approximation to the spatial variation of the solution of the full nonlinear system. The above examples have at most two eigenvalues with positive real parts. The method, however, also works in cases where there are more than two eigenvalues with positive real parts. The analysis then predicts a superposition of several modes. We have compared the predictions of the analysis with the numerical solution of the corresponding linear reaction diffusion system for several cases of this type and found them to be in very good agreement. This study, however, also highlights the shortcoming of linear analysis in that if more than one eigenfunction grows the analysis cannot determine if the final pattern of the full nonlinear system will be a combination of eigenfunctions or dominated by one eigenfunction.

Example 3. If we take the lowest order FDA ($M = 1$) we find from (42) that the temporal growth rate λ is given by

$$2\lambda = k_{11} + k_{22} - v\pi^2 \pm [(k_{11} + k_{22} - v\pi^2)^2 - 4(k_{11}k_{22} - k_{12}k_{21} - k_{22}v\pi^2)]^{1/2}. \quad (45)$$

The condition $k_{11} + k_{22} < 0$ (from Sect. 2) implies that $k_{11} + k_{22} - v\pi^2 < 0$, but the condition $k_{11}k_{22} - k_{12}k_{21} > 0$ does not necessarily imply that $k_{11}k_{22} - k_{12}k_{21} - k_{22}v\pi^2 > 0$, unless $k_{22} < 0$. If $k_{22} > 0$, then for large enough v , $k_{11}k_{22} - k_{12}k_{21} - k_{22}v\pi^2 < 0$ and the larger of the two roots (45) is positive. It may thus be possible for a uniform steady state which is stable in the standard case of zero flux boundary conditions on both species to be driven linearly unstable by boundary conditions of the form (38). This may be illustrated for the glycolysis model for the D_1N case at $L = 0.045$. For these parameter values the linear analysis predicts that the standard Turing system (with zero flux boundary conditions on both species) is stable, a result confirmed by numerically solving the partial differential equation system but that the case with boundary conditions (38) should have a growing eigenfunction which at FDA of dimension 1 is

$$\begin{pmatrix} \xi_1 \\ \xi_2 \end{pmatrix} = C_1 \begin{pmatrix} -0.387 \sin \pi\zeta \\ 1 \end{pmatrix} e^{0.694\tau}. \quad (46)$$

At the two-dimensional approximation another positive eigenvalue appears and the FDA is now

$$\begin{pmatrix} \xi_1 \\ \xi_2 \end{pmatrix} = C_1 \begin{pmatrix} -0.387 \sin \pi\zeta \\ 1 \end{pmatrix} e^{0.696\tau} + C_2 \begin{pmatrix} -0.082 \sin 2\pi\zeta \\ \cos \pi\zeta \end{pmatrix} e^{0.219\tau}. \quad (47)$$

At the 16-dimensional approximation these solutions have converged to

$$\begin{pmatrix} \xi_1 \\ \xi_2 \end{pmatrix} = C_1 \begin{pmatrix} -0.376 \sin \pi\zeta - 0.020 \sin 3\pi\zeta - 0.004 \sin 5\pi\zeta + \mathcal{O}(10^{-4}) \\ 1 + 0.057 \cos(2\pi\zeta) + 0.004 \cos(4\pi\zeta) + \mathcal{O}(10^{-4}) \end{pmatrix} e^{0.752\tau} \\ + C_2 \begin{pmatrix} -0.081 \sin(2\pi\zeta) - 0.009 \sin(4\pi\zeta) + \mathcal{O}(10^{-4}) \\ \cos \pi\zeta + 0.006 \cos 3\pi\zeta + \mathcal{O}(10^{-4}) \end{pmatrix} e^{0.242\tau}. \quad (48)$$

Equation (45) also predicts that the value of the positive λ will increase as v decreases. This is borne out by solving the generalized eigenvalue problem and also the linear partial differential equation system.

This example shows that boundary conditions can drive a reaction-diffusion system, which would otherwise be stable, to become unstable and exhibit spatial pattern. This is to be expected intuitively because u is the inhibitor, thus setting it to zero on the boundary will tend to allow the activator to grow unbounded in a linear system.

The above examples show that even very crude, low dimensional, finite dimensional approximations provide a reasonably accurate solution to the infinite dimensional generalized eigenvalue problem (42). If we choose parameters which predict the growth of higher modes for the standard Turing system with zero flux boundary conditions on both species we find that higher dimensional FDA need to be used in order to obtain sufficient accuracy.

All the above analysis could have been carried out by taking the inner product with cosine in (42). The results are in good agreement with the above.

A.2 Further analysis

We can gain some insight into the connection with the Neumann problem as follows. Note that the system (42) may be reduced by eliminating A_m to

$$\sum_{n=0}^{\infty} [(\lambda + v(m\pi)^2 - k_{11})(\lambda + v\delta(n\pi)^2 - k_{22}) - k_{12}k_{21}] \alpha_{nm} B_n = 0 \quad (49)$$

for $m = 1, 2, 3, \dots$

This may be written as

$$\sum_{n=0}^{\infty} \{ \lambda^2 + [v(m\pi)^2 + \delta v(n\pi)^2 - \text{trace } K] \lambda + \delta v^2(m\pi)^2(n\pi)^2 - [k_{11} v(m\pi)^2 + k_{22} v(n\pi)^2] + \det K \} B_n \alpha_{nm} = 0,$$

which shows the connection with the Neumann problem more clearly, for in that case (9),

$$v(m\pi)^2 + \delta v(n\pi)^2 \rightarrow (m\pi)^2 \text{ trace } D.$$

As $\alpha_{nm} = 0$ for $n + m = 2p$, the infinite system represented by (49) can be written as

$$\Omega(\lambda) \mathbf{B} = \begin{bmatrix} \Omega_1(\lambda) & 0 \\ 0 & \Omega_2(\lambda) \end{bmatrix} \begin{bmatrix} \mathbf{B}_e \\ \mathbf{B}_o \end{bmatrix}.$$

Here $\mathbf{B}_e = (\mathbf{B}_0, \mathbf{B}_2 \dots)^T$ and $\mathbf{B}_o = (\mathbf{B}_1, \mathbf{B}_3 \dots)^T$. Thus $\det \Omega(\lambda) = \det \Omega_1(\lambda) \det \Omega_2(\lambda)$ and the eigenvectors decompose into those with only $B_j \neq 0$ for j even and those with only $B_j \neq 0$ for j odd. This explains the form of the eigenfunctions in Examples 1–3.

A.3 Location of bifurcation points

The above analysis can be used to locate bifurcation points as a certain parameter p is varied using the method of bisection as follows: we choose a low dimensional FDA, a value of the parameter p say, p_1 at which all eigenvalues have real part negative and another value p_2 at which at least one eigenvalue has positive real part. Assume, without loss of generality, that $p_2 > p_1$. Clearly, an odd number of eigenvalues must cross the axis in (p_1, p_2) . By examining the signs of the eigenvalues at the midpoint $(p_1 + p_2)/2$ of the interval we can easily determine in which half of the interval the bifurcation point lies. We can continue this procedure to find the bifurcation point to the required degree of accuracy. By going to a higher dimensional FDA we may obtain a more accurate value of the parameter at the bifurcation point. The results of this method agree closely with those from the package AUTO. For example, in Fig. 10 bifurcation points occur at $L = 0.216$ and $L = 0.226$. The above procedure predicts bifurcation at $L = 0.219$ and 0.228 .

B Appendix

B.1 Numerical methods

To investigate the steady state solutions of (21) we discretise the system using central differences:

$$\begin{aligned} \frac{D_1}{h^2\omega L^2}(u_{j+1} - 2u_j + u_{j-1}) + f(u_j, v_j) &= 0 \\ \frac{\delta D_1}{h^2\omega L^2}(v_{j+1} - 2v_j + v_{j-1}) + g(v_j, v_j) &= 0 \end{aligned} \tag{50}$$

where $Nh = 1$, $N \in \mathbb{N}$, $u_j = u(jh)$, and $v_j = v(jh)$ $j = 1, 2, \dots, N - 1$. This is a system of $2N - 2$ equations with $2N + 2$ unknowns. To get the remaining four equations, we use central differences for the first derivatives at the boundary and introduce the ‘fictitious’ points $\zeta_{-1} = -h$, and $\zeta_{N+1} = (N + 1)h$, in order to write the discretised boundary conditions as

$$\begin{aligned} \frac{\theta_1}{2h}(u_{-1} - u_1) + (1 - \theta_1)u_0 - \theta_3 u^s &= 0 \\ \frac{\theta_2}{2h}(v_{-1} - v_1) + (1 - \theta_2)(v_0 - \theta_3 v^s) &= 0 \\ \frac{\theta_1}{2h}(u_{N+1} - u_{N-1}) + (1 - \theta_1)(u_N - \theta_3 u^s) &= 0 \\ \frac{\theta_2}{2h}(v_{N+1} - v_{N-1}) + (1 - \theta_2)(v_N - \theta_3 v^s) &= 0. \end{aligned} \tag{51}$$

By substituting (51) into (50) with $j = 0$ and $j = N$, we get

$$\begin{aligned} \frac{2\theta_1 D_1}{h^2\omega L^2}(u_1 - u_0) - \frac{2D_1}{h\omega L^2}(1 - \theta_1)(u_0 - \theta_3 u^s) + \theta_1 f(u_0, v_0) &= 0 \\ \frac{2\theta_2 D_2}{h^2\omega L^2}(v_1 - v_0) - \frac{2D_2}{h\omega L^2}(1 - \theta_2)(v_0 - \theta_3 v^s) + \theta_2 g(u_0, v_0) &= 0 \\ \frac{2\theta_1 D_1}{h^2\omega L^2}(u_{N-1} - u_N) - \frac{2D_1}{h\omega L^2}(1 - \theta_1)(u_N - \theta_3 u^s) + \theta_1 f(u_N, v_N) &= 0 \\ \frac{2\theta_2 D_2}{h^2\omega L^2}(v_{N-1} - v_N) - \frac{2D_2}{h\omega L^2}(1 - \theta_2)(v_N - \theta_3 v^s) + \theta_2 g(u_N, v_N) &= 0. \end{aligned} \tag{52}$$

We solved the discretized steady state problem (50) and (52) with AUTO [6]. This program detects bifurcation from a given steady state as the bifurcation parameter is varied and can calculate solutions and their stability by continuation along bifurcating branches. Throughout we fixed $D_1 = 10^{-5} \text{ cm}^2/\text{sec}$, $\omega = 0.01 \text{ sec}^{-1}$, $\delta = 0.14$, $\beta = 1.0$, $\kappa = 0.001$, and $N = 40$. As a check on the solutions, we computed several solutions to the evolution equations corresponding to (21), with appropriate boundary conditions, using the method of lines and Gear’s method. In all cases, the steady state solutions obtained by AUTO and those obtained from the evolution equations were similar.

In the cases NN and $D_1 D_1$, the uniform steady state of the full system is simply (u^s, v^s) . However, for the cases $ND_0, D_0 N, D_0 D_0$ the problem of initially specifying a steady state for AUTO is more difficult. The starting solutions were determined by one of the following methods.

(i) Solve the corresponding time evolution problem and use the resulting steady state solution as a starting point for AUTO. For example, we used such a method to obtain the solution to the D_0N case at $L = 0.1$ and then continued the solution with AUTO. The bifurcation diagram thus derived is shown in Fig. 15.

(ii) Use a homotopy from a known solution for a different set of boundary conditions. This may be done in several ways. For example, to find an initial steady state for the ND_0 case we used two different homotopy methods. For both methods, θ_1 , was set to 1 so that u satisfied homogeneous Neumann conditions. In the first method we introduced a parameter p and set the boundary values of v , namely $v(0)$ and $v(N)$, equal to p for a fixed value of L . The parameter p was initially set equal to v^s and then used as the continuation parameter. When p reaches zero, we have a steady state solution to the ND_0 problem. This solution may then be continued in L to investigate its bifurcation structure under these boundary conditions.

The second method used θ_2 as the homotopy parameter in Eq. (22). The parameter was initially set to 1 with the starting solution set at (u^s, v^s) . Continuing in θ_2 with AUTO until $\theta_2 = 0$ gives a homotopy between the homogeneous Neumann and homogeneous Dirichlet conditions for v .

Note that the starting solution for the homotopy in the second method need not necessarily be (u^s, v^s) . One may start with a spatially heterogeneous steady state obtained from the NN case. Several cross checks were carried out with these different homotopy procedures and the solutions were found to agree.

References

1. Ashkenazi, M., Othmer, H. G.: Spatial patterns in coupled biochemical oscillators. *J. Math. Biol.* **5**, 305–350 (1978)
2. Babloyantz, A., Bellemans, A.: Pattern regulation in reaction-diffusion systems – the problem of size invariance. *Bull. Math. Biol.* **47**, 475–487 (1985)
3. Benson, D. L., Sherratt, J. A., Maini, P. K.: Diffusion driven instability in an inhomogeneous domain. *Bull. Math. Biol.* **55**, 365–384 (1993)
4. Benson, D. L., Maini, P. K., Sherratt, J. A.: Pattern formation in heterogeneous domains. In: Othmer, H. G., Maini, P. K., Murray, J. D. (eds.) *Experimental and Theoretical Advances in Biological Pattern Formation*. London: Plenum 1993
5. Brümmer, F., Zempel, G., Buhle, P., Stein, J.-C., Hulser, D. F.: Retinoic acid modulates gap junction permeability: a comparative study of dye spreading and ionic coupling in cultured cells. *Exp. Cell Res.* **196**, 158–163 (1991)
6. Castets, V., Dulos, E., De Kepper, P.: Experimental evidence of a sustained standing Turing-type nonequilibrium chemical pattern. *Phys. Rev. Lett.* **64**(24), 2953–2956 (1990)
7. Child, C. M.: *Patterns and Problems of Development*. University of Chicago Press, 1941
8. Conway, E., Hoff, D., Smoller, J.: Large time behavior of solutions of nonlinear reaction diffusion equations. *SIAM J. Appl. Math.* **35**(1), 1–16 (July 1978)
9. Crick, F. H.: Diffusion in embryogenesis. *Nature* **225**, 420–422 (1970)
10. Dillon, R., Othmer, H. G.: Control of gap junction permeability can control pattern formation in limb development. In: Othmer, H. G., Maini, P. K., Murray, J. D. (eds.) *Experimental and Theoretical Advances in Biological Pattern Formation*. London: Plenum 1993
11. Doedel, E.: AUTO: Software for continuation and bifurcation problems in ordinary differential equations. Technical report, California Institute of Technology, 1986
12. Driesch, H.: *Entwicklungsmechanische Studien*. *Z. Wiss. Zool.* **53**, 160–184 (1892)
13. Driesch, H.: *Entwicklungsmechanische Studien*. *Z. Wiss. Zool.* **55**, 3–61 (1893)
14. Epstein, I. R., Lengyel, I., Kádár, S., Kagan, M., Yokoyama, M.: New systems for pattern formation studies. *Physica A*, **188**, 26–33 (1992)

15. French, V., Bryant, P. J., Bryant, S. V.: Pattern regulation in epimorphic fields. *Science* **193**, 969–981 (1977)
16. Goodwin, B. C., Kauffman, S. A.: Spatial harmonics and pattern specification in early *Drosophila* development. Part I. Bifurcation sequences and gene expression. *J. Theor. Biol.* **144**, 303–319 (1990)
17. Hunding, A., Sorensen, P. G.: Size adaptation of Turing prepatterns. *J. Math. Biol.* **26**, 27–39 (1988)
18. Lacalli, T. C., Harrison, L. G.: The regulatory capacity of Turing's model for morphogenesis with application to slime moulds. *J. Theor. Biol.* **70**, 273–295 (1978)
19. Lengyel, I., Epstein, I.R.: A chemical approach to designing Turing patterns in reaction-diffusion systems. *Proc. Natl. Acad. Sci.* **89**, 3977–3979 (1992).
20. Meinhardt, H.: *Modes of Biological Pattern Formation*. London: Academic Press 1982
21. Moler, C. B., Stewart, G. W.: An algorithm for generalized matrix eigenproblems. *SIAM J. Numer. Anal.* **10**, 241–256 (1973)
22. Murray, J. D.: *Mathematical Biology*. Berlin Heidelberg New York: Springer 1989
23. Othmer, H. G.: *Interactions of Reaction and Diffusion in Open Systems*. PhD thesis, Minneapolis: University of Minnesota 1969
24. Othmer, H. G.: Current problems in pattern formation. In: Levin, S. A. (ed.) (Some mathematical questions in biology VIII. *Lect. Math. Life Sci.*, vol. 9, pp. 57–85) Providence, RI: Am. Math. Soc. 1977
25. Othmer, H. G.: Applications of bifurcation theory in the analysis of spatial and temporal pattern formation. In: Gurel, O., Rössler, O. K. (eds.) *Bifurcation theory and applications in scientific disciplines*, pp. 64–77. New York: New York Academy of Sciences 1979
26. Othmer, H. G.: Synchronized and differentiated modes of cellular dynamics. In: Haken, H. (eds.) *Dynamics of Synergetic Systems*. Berlin Heidelberg New York: Springer 1980
27. Othmer, H. G.: The interaction of structure and dynamics in chemical reaction networks. In: Ebert, K. H., Deuflhard, P., Jäger, W. (eds.) *Modelling of Chemical Reaction Systems*, pp. 1–19 Berlin Heidelberg New York: Springer 1981
28. Othmer, H. G., Aldridge, J.: The effects of cell density and metabolite flux on cellular dynamics. *J. Math. Biol.* **5**, 169–200 (1978)
29. Othmer, H. G., Pate, E. F.: Scale invariance in reaction-diffusion models of spatial pattern formation. *Proc. Nat. Acad. Sci.* **77**, 4180–4184 (1980)
30. Othmer, H. G., Scriven, L. E.: Interactions of reaction and diffusion in open systems. *Ind. Eng. Chem. Fund.* **8**, 302–315 (1969)
31. Ouyang, Q., Swinney, H. L.: Transition from a uniform state to hexagonal and striped patterns. *Nature* **352**, 610–612 (1991)
32. Pate, E., Othmer, H. G.: Applications of a model for scale-invariant pattern formation in developing systems. *Differentiation* **28**, 1–8 (1984)
33. Pearson, J. E., Horsthemke, W.: Turing instabilities with nearly equal diffusion coefficients. *J. Chem. Phys.* **90**(3), 1588–1599 (1989)
34. Turing, A. M.: The chemical basis of morphogenesis. *Philos. Trans. R. Soc. Lond. Ser. B* **237**, 37–72 (1952)
35. Ward, R. C.: The combination shift QZ algorithm. *SIAM J. Numer. Anal.* **12**, 835–853 (1975)
36. Wolpert, L.: Positional information and the spatial pattern of cellular differentiation. *J. Theor. Biol.* **25**, 1–47 (1969)
37. Wolpert, L.: Positional information and pattern formation. *Curr. Top. Dev. Biol.* **6**, 183–224 (1971)
38. Wright, D. A., Lawrence, P. A.: Regeneration of the segment boundary in *Oncopeltus*. *Dev. Biol.* **85**, 317–327 (1981)